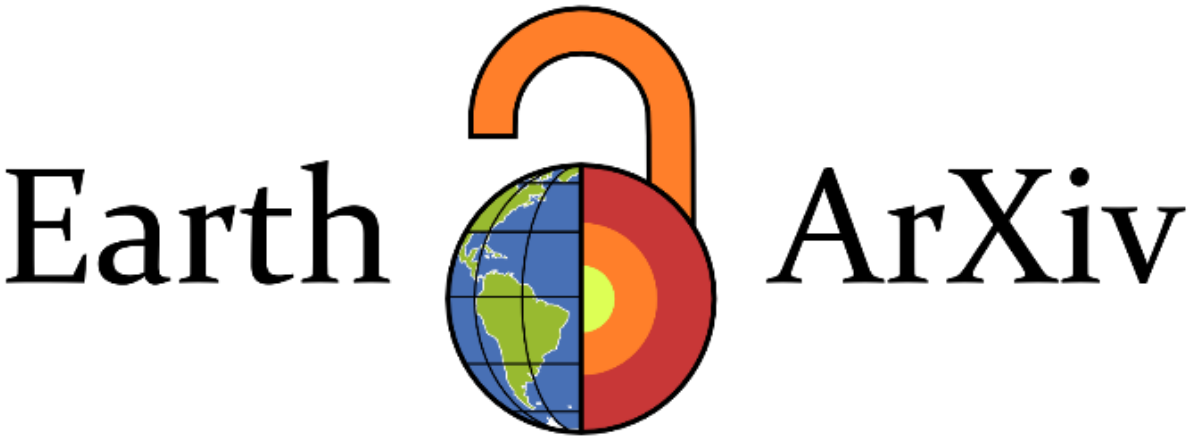

Chemical and meteorological drivers of ozone extremes during the 2019 UK summer heatwaves

Andrea Mazzeo[1*] and Ryan Hossaini[1]

* a.mazzeo@lancaster.ac.uk

[1]Lancaster Environment Centre, Lancaster University, UK.

Keywords: *Ozone, heatwaves, UK, air pollution, biogenic emissions, isoprene*

Abstract: Heatwave-associated air pollution episodes are increasingly recognized as a public health threat. Studies have observed a positive correlation between extreme temperature and extreme surface ozone concentrations. However, the underpinning chemical and physical drivers and their interconnections are not well quantified and may vary across regions and individual heatwave events. The 2019 UK summer offers a compelling case study, as three distinct heatwave events occurred, with record-breaking temperatures and widespread ozone exceedances above health-relevant thresholds. Here, we use the WRF-Chem chemistry-transport model to investigate the drivers of elevated UK ozone during the three heatwaves. We show WRF-Chem simulates observed ozone and temperature well over the full summer, including heatwave-associated ozone enhancements. Net chemical ozone production increased markedly over much of the UK, including enhancements of +4.2 ppb/hr relative to non-heatwave periods in the South-East of England (reaching 8.20 ppb/hr at midday). Large enhancements in biogenic isoprene emissions (up to 200% in some areas) during the heatwaves are shown to broadly correlate with formaldehyde enhancements observed from TROPOMI satellite data. Meteorologically, the heatwaves were characterised by low ventilation of the planetary boundary layer, affecting pollutant dispersal. Sensitivity analysis also demonstrates that the import of ozone and its precursors from outside of the UK was a key factor in elevating daily maximum 8-hour running mean (MDA8) ozone above the health-relevant 100 μg/m^3 threshold. We conclude that as the frequency and intensity of heatwaves increases due to climate change, more extensive local monitoring of isoprene and other natural emissions is needed to characterise changes, and that efforts to reduce European-wide ozone precursor emissions are required to lower extreme surface ozone over the UK.

1. Introduction

Heatwaves (prolonged periods of exceptionally hot weather) are events of increasing research and policy focus owing to the public health and broader environmental challenges they pose. The precise definition of a heatwave varies with context and by country. In the UK, according to the Met Office a ‘heatwave’ is a period with at least three consecutive days with daily maximum temperature exceeding a regionally varying threshold, in the range 25-28 °C [1]. Heatwaves impact the biosphere in a myriad of direct and indirect ways, including well established harmful effects of extreme heat on human health, especially among vulnerable groups [2], along with adverse effects on terrestrial and marine ecosystems [3]. While heatwaves are a well-recognised public health hazard in their own right, growing evidence highlights a compounding risk from the co-occurrence of extreme temperature and extreme air pollution events [4, 5]. Due to climate change, the frequency and intensity of heatwaves have increased in Europe and elsewhere [6] and are projected to continue to do so [7], potentially amplifying the "climate penalty" on air quality [8].

Heatwaves are identified as being associated with elevated surface ozone (O_3) concentrations in many regions, including the USA [9], Europe [10], and China [11]. At the surface, ozone is an important air pollutant that has negative impacts on human health and vegetation. Across Europe

alone, ozone exposure is estimated to have been responsible for some 63,000 premature deaths in the year 2023 [12]. While studies have long established a positive correlation between temperature and ozone [13, 14], the underpinning process, or combination of processes, that cause the relationship remains unclear. During heatwaves, factors such as increased photochemical activity, altered dry deposition, emissions of volatile organic compounds (VOCs), and stagnation of air masses – related to synoptic weather conditions – may significantly enhance ozone levels [15-17]. The net ozone-temperature response thus likely reflects a complex interaction of both meteorological and chemical factors, with the individual components potentially varying with region and time. An improved understanding of the relationship between extreme temperature and ozone during heatwaves is crucial, as this connection provides an aggravating effect on public health [4, 18-20].

In the UK, analysis of surface ozone measurements reveals a long-term decline in the probability of extreme ozone events since the 1990s [21, 22], attributed to local and regional decreases in ozone precursor emissions (principally NO_x) over this period [23]. However, these studies also highlight the positive correlation between temperature and ozone, and heatwaves specifically are identified as a driver of episodic extreme ozone events [24]. While empirical observations have thus far established a positive correlation between ozone and temperature over the UK [21], they cannot alone detangle the underpinning processes and their complexities. This is where advanced modelling approaches, such as the use of chemistry-transport models (CTMs), can offer valuable insights. By simulating the meteorological and chemical processes that govern ozone formation and loss during heatwaves, these models allow for a more comprehensive understanding of the underlying processes. They also allow for a wider spatial characterisation of extreme episodes in areas that extend beyond fixed-location measurement networks.

The prominent 2003 European heatwave resulted in an estimated 2,045 excess deaths in England and Wales, with the highest number concentrated in the South-East of England, particularly London [25]. Although carrying significant uncertainty, a portion of these total excess deaths (21-38%) have been attributed to elevated ozone and particulate matter (PM) pollution during the heatwave [26]. The effects of the severe 2003 heatwave on air quality are relatively well studied using both measurements and models. Field measurements during the event showed complex ozone photochemistry, highlighting a significant role for biogenic isoprene emissions in increasing ozone concentrations [27]. In addition to biogenic VOC emissions, Vieno (2010) [17] used the EMEP4UK model to demonstrate that other processes, including supressed ozone dry deposition, likely contributed to the elevated ozone during the 2003 heatwave. The long-range transport of ozone from continental Europe to the UK was likely an additional important factor [28]. Investigations of air quality during other prominent heatwaves reveal similar complexity. For example, the Summer 2018 heatwave [29] saw elevated lower tropospheric and surface level ozone, attributed to a mixture of both meteorological and chemical factors [30]. In-situ isoprene measurements at Wytham Woods in the UK showed an increase of 400% during the 2018 heatwave, providing further strong evidence for an important role of biogenic VOC emissions [31].

The UK summer of 2019 presents a relatively recent and compelling case study that is thus far understudied. Three distinct heatwave events occurred between June and August 2019, marked by at the time record-breaking temperatures – with a peak of 38.7°C recorded in Cambridge [32, 33] – and widespread ozone exceedances above 100 $\mu g/m^3$ (8-hr mean) observed at more than 40 air quality stations in both urban and rural areas. In this study, we investigate the meteorological and chemical drivers of elevated ozone during the 2019 UK summer heatwaves. To achieve this, we combine numerical modelling from the WRF-Chem chemistry-transport model (CTM) [34] with analysis of various observational data. The paper is structures as follows. In Section 2, we describe the observations used, the configuration of WRF-Chem, and our experimental design. An evaluation of WRF-Chem for the full summer 2019 period is performed in Section 3. Our main results are presented in Section 4, including a measurement and model characterisation of ozone behaviour during the three heatwaves (Sect. 4.1), examination of the ozone budget, including dry deposition (Sect. 4.2), and investigations into the effects of biogenic VOC emissions (Sect. 4.3) and synoptic meteorological conditions, including the import of ozone and precursors to the UK (Sect. 4.4).

2. Materials and Methods

2.1 Analysed period and meteorological context

The period chosen for the WRF-Chem simulation is the entirety of summer 2019 (from the 1st of June to the 31st of August) when 3 'heatwaves' occurred (**Table S1**). During this summer, two 'Level 3' heatwave alerts were issued by the UK Met Office. Recall, the Met Office defines a heatwave when daily maximum temperature exceeds a regionally varying threshold (in the range 25-28°C) on at least three consecutive days. A further heatwave was defined according to the UK Health Security Agency (UKHSA) heatwave definition of days when the mean Central England Temperature (CET) is greater than 20°C [35].

2.1.1 June heatwave

The June heatwave defined according to the UKHSA definition occurred between the 28th and 30th of the month. It was characterized mainly by warm and humid weather and prevalent high pressure. Significant convective activity (e.g., thunderstorms and heavy rain) resulting in weather alerts was observed during the month, in particular between the 10th - 15th of the month. The 29th June was the day with the highest national temperature recorded, occurring at Heathrow and Northolt (Great London) and reaching 34°C [36]. No cumulative excess deaths were observed in the 0 – 64 years age group or in the 65+ years old group in England [37].

2.2.2 July heatwave

The July heatwave (21st to the 28th) was characterised by short and exceptionally hot temperature. The peak of the heatwave saw a highest national temperature of 38.7°C recorded at the Cambridge Botanic Garden in the East of England. At the time, this peak set a record for the all-time UK hottest temperature [38]. This heatwave occurred alongside high pressure developed over Western Europe that brought increasingly warm air from south to North onto the British Isles. According to Public Health England [37], during the July heatwave, an estimated 572 (390-754, 95% CI) excess deaths occurred above the baseline for all-cause mortality in individuals aged 65 years and older in England. The regions most impacted included South-East England (137 excess deaths, 95% CI), the East of England (116 excess deaths, 95% CI), and London (74 excess deaths, 95% CI).

2.2.3 August heatwave

The August heatwave (23rd to the 29th) was characterised by a prolonged period of hot temperatures. Highest temperatures were recorded at Heathrow (London) reaching 33.3°C on the 25th, 33.2°C on the 26th and 33.4°C on the 27th setting a record of high temperature during the late August bank holiday [39]. The August heatwave occurred during similar synoptic meteorological conditions to those in July (Section 2.1.2). During the August heatwave, a cumulative total of 320 (150-490, 95% CI) excess deaths were reported in 65+ years old demographic [37]. The regions most impacted included South-East England (105 excess deaths, 95% CI), the East of England (88 excess deaths, 95% CI), and London (108 excess deaths, 95% CI).

2.2 Ozone and temperature observations

Observed hourly surface concentrations of ozone (O_3) and temperature at 2 metres (T_{2m}) have been taken from the UK's Automatic Urban and Rural Network (AURN) [40] and from the Met Office's Integrated Data Archive System (MIDAS) weather network [41], respectively. The former is the UK's largest automatic monitoring network for air quality and includes observations at high temporal resolution for a variety of gaseous species and aerosols. The latter is a global dataset providing weather measurements, also at high temporal resolution (hourly). Here, a subset of stations located in the UK have been used. A total of 104 observation sites from AURN (urban and rural background) and 126 weather stations from the MIDAS dataset have been used to evaluate the performance of the WRF-Chem simulation of summer 2019.

AURN sites were paired with the closest MIDAS site to provide concurrent hourly records of both ozone and T_{2m} over our Summer 2019 study period (**Figure 1**). The relationship between ozone and T_{2m} has been analysed following the methodology used by Bloomer (2009) [13] and from this a

"climate penalty factor" (CPF) is calculated. The CPF is here defined as the slope of the linear regression line relating ozone with T_{2m}. It shows how much the former changes in relation to increases in the latter (i.e., μg/m^3 per °C). Previous studies have highlighted a roughly linear relationship between 19°C and 37°C between the two variables though there are few UK-focussed studies [13, 14, 42].

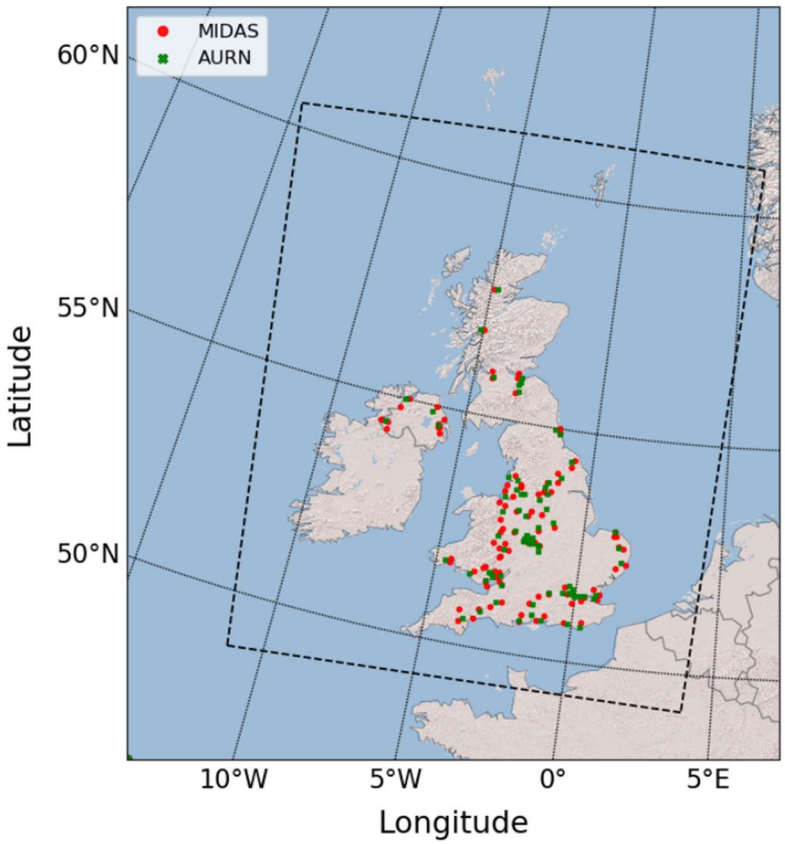

Figure 1. Location of the filtered subset of observation points from the AURN (green) and MIDAS (red) networks used in the analysis of the ozone-temperature relationship. The dashed black line defines the borders of the internal domain used for the WRF-Chem simulations with a spatial resolution of 5×5 km

2.3 Modelling system

2.3.1 WRF-Chem

The WRF-Chem CTM [34] was used to simulate meteorology and chemistry during the UK Summer of 2019. A regional model, WRF-Chem couples advanced weather prediction capabilities with detailed atmospheric chemistry, making it a useful tool to explore the interactions between temperature, emissions, and the photochemistry that govern ozone production and loss during heatwaves. The model's ability to incorporate real-world emissions data for both anthropogenic and biogenic sources, combined with its high spatial and temporal resolution, enables precise simulations of ozone behaviour under extreme weather conditions [43]. Furthermore, WRF-Chem has been shown to effectively simulate key meteorological phenomena such as air mass stagnation, boundary layer dynamics, and temperature inversions, which are critical meteorological drivers of elevated ozone levels during heatwaves [44, 45].

2.3.2 Nested grid

A system of two domains at different spatial resolution were chosen for our simulations over the UK (**Figure 1**). The first domain with a spatial resolution of 10×10 km covers the UK and a great part of the European continent (not shown). The nested domain is centred on the UK and has spatial resolution of 5×5 km (**Figure 1**, dashed black line). Both domains have 30 vertical levels with 9 levels

located below 1 km of height and with the first level at 20 m from the ground. The vertical domain extends up to 50 hPa.

2.3.3 Model configuration and boundary conditions

The WRF-Chem configuration chosen follows the one adopted by Crippa (2017) [46] who performed sensitivity tests with the model comparing how different configurations simulate regional ozone over Europe. The individual options and related numerical codes for the WRF-Chem 'namelist.input' files are provided in **Table 1**. Full details of the configuration can be found in Crippa (2017) [46]. The chemical mechanism used is the second-generation Regional Acid Deposition Model (RADM2) mechanism for regional air quality modelling [47]. RADM2 includes 63 chemical species and 136 gas-phase reactions. It includes isoprene oxidation and uses a "lumped molecule" technique for VOCs in which similar organic compounds are grouped. The mechanism has been extensively adopted for regional simulations of ozone and aerosols at different spatial resolution [46, 48-50].

Table 1: WRF-Chem configuration used for the simulations. N represents the model's namelist variable numbers to activate the options.

Parameter	Option	N	Reference
Micro physics options	Eta (Ferrier) Scheme	5	[51]
Land Surface processes	Noah Land surface model	2	[52]
Land use data set	USGS 24-category land use	-	
Cumulus Convection	Grell 3-D scheme	5	[53]
Surface Layer	Eta Monin-Obukhov (Janjic)	2	[54, 55]
Boundary Layer Physics	Mellor-Yamada-Janjic (MJY) TKE	2	[55, 56]
Short wave radiation	Goddard shortwave scheme	2	[57]
Long wave radiation	RRTMG	1	[58]
Urban Physics	Building Environment Param. (BEP)	2	[59]
IC/BC (meteorology)	ERA5 Re-analysis	-	[60]
IC/BC (chemistry)	CAM-Chem	-	[61]
Grid nudging	Analysis Nudging (FDDA)	1	[62]
Anthropogenic Emissions	NAEI (UK) – CAMSv3.1 (Elsewhere)	-	[63]
Biogenic Emissions	Online using MEGANv2.1	3	[64]
Biomass burning Emiss.	Fire Inventory from NCAR v2 (FINN)	-	[65]
Chemical Mechanisms	RADM2	106	[47]

Meteorological initial conditions and lateral boundary conditions (IC/BC) to drive WRF-Chem were derived from the European Centre for Medium-Range Weather Forecast (ECMWF) ERA5 Reanalysis [60]. These IC/BC are created using forecasts at 31 km resolution (one-fourth the spatial resolution of the operational model). They integrate 137 hybrid sigma-pressure levels in the vertical, up to 0.01 hPa. The choice of IC/BC data can have a significant impact on both meteorological patterns and on regional air quality. The adoption of ECMWF-based fields in this work is motivated by previous studies that have optimised WRF's configuration for UK simulations [66].

As our study is a hindcast analysis, it is important that the model meteorology is as realistic as possible to permit meaningful comparisons to ozone observations. Grid nudging has therefore been

applied every 6 h (*grid_fdda =1,1,*), with nudging coefficients defined for U and V wind components, temperature (T) and water vapour mixing ratio (Q) [62]. The nudging process constrains the values of these variables calculated by WRF (e.g., U, V, T and Q) to the ECMWF reanalysis data.

Initial and lateral boundary conditions of chemical composition have been taken from the outputs of a CAM-chem simulation [61]. These model outputs were generated using the chemistry mechanism of the Community Earth System Model version 2 (CESM2) and are intended to be used as boundary conditions for regional modelling. The CAM-chem outputs were generated at a horizontal resolution of 0.9°×1.25° and with 56 vertical levels. Meteorology used to drive CAM-chem came from MERRA2 reanalysis [67].

For an analysis of the ozone budget during the heatwave we used diagnostic variables included in WRF-Chem, including tendencies due to net chemical production (*chem_o3*), horizontal and vertical advection (*hadv_o3, vadv_o3*) via wind patterns, vertical mixing (*vmix_o3*) via boundary layer turbulence, and convective activity (*conv_o3*), such as thunderstorms. These variables are part of an integrated process rate module developed by Jeffries and Tonnesen (1994) [68] aimed to disentangle the interplay between physical and chemical mechanisms affecting ozone production during air pollution episodes. These tendencies have been demonstrated to be powerful diagnostic tools in highlighting the drivers of ozone formation and transport during extreme heatwave events [69].

2.3.4 Emissions

Anthropogenic emissions (e.g. NO_x, CO, VOCs etc.) used as input in our WRF-Chem simulations were taken from two inventories. The National Atmospheric Emission Inventory (NAEI) provides the most up-to-date estimates of anthropogenic emissions for the UK at a spatial resolution of 1×1 km [63]. The NAEI emissions for 2019 were used to cover all UK (England, Scotland, Wales and Northern Ireland) emissions. The CAMSv3.1 regional emission inventory (hereafter CAMS) [70] provides emissions for the whole of Europe at a spatial resolution of 10×10 km and were used to cover the emissions in other parts of the WRF-Chem domain not provided by the NAEI.

Both inventories provide detailed emission data divided by species, including gaseous pollutants (e.g. NO_x, NH_3, SO_2, VOCs, CO) and aerosols (PM_{10}, $PM_{2.5}$). Emission annual totals are divided by sector according to the UNECE/CORINAIR SNAP 94 Version 1.0 nomenclature [71]. The NAEI and CAMS inventories have different spatial resolution (1×1 km vs 10×10 km, respectively) but the same temporal resolution (annual totals) and for this reason have been spatially and temporally allocated on the final grids of the model's domain independently using the HERMESv3 tool [72, 73]. HERMES is an open-source, Python-based, parallel, stand-alone and multi-scale atmospheric emission modelling framework. It allows emissions data to be projected onto different CTM grids, including WRF-Chem [74]. HERMES estimates emission fluxes on the basis of reported EMEP/EEA methodologies for air pollutant emission inventories and has been used for multiple studies in air quality research from regional [75-77] to urban level [78, 79] and for air quality forecasting [80].

Biogenic emissions were simulated online in WRF-Chem using the Model of Emissions of Gases and Aerosols from Nature (MEGAN) version 2.1 [64, 81]. Briefly, MEGAN calculates biogenic emissions based on Plant Functional Type (PFT) information (percentage of broadleaf, needle leaf, shrubs, herbaceous biota), Leaf Area Index (LAI), air temperature and short-wave radiation. Temperature and radiation fields are taken directly from the WRF-Chem meteorology. Biogenic emissions from MEGAN of the following species were included in our simulations: isoprene, monoterpenes, oxygenated compounds, sesquiterpenes and nitrogen oxide.

Biomass burning emissions were prescribed from the Fire INventory from NCAR (FINN) dataset [65]. Briefly, these emissions are available at high spatial resolution (1×1 km) and are based on remote sensing observations of fires (wildfires, agricultural fires etc.) and land cover, along with species-specific emission factors. Annual emissions of the following species were included in our simulations: non-methane volatile organic compounds (NMVOCs), CO, NO, NO_2, NH_3, SO_2, and organic and black carbon (OC, BC) aerosols.

2.4 Simulations and sensitivity experiments

Three WRF-Chem simulations were performed, each covering the 3-month period between the 1st of June and 31st August 2019. A 10-day spin-up period was applied to the simulations before the above analysis period. The BASE run included all the processes detailed in Section 2.3 above. To investigate the importance of different processes in affecting ozone during the heatwave events, several sensitivity tests were conducted. Run noISOP was identical to the BASE run but excluded biogenic isoprene emissions. Run fixBC was identical to the BASE run but excluded the time-dependent chemical boundary conditions from the parent domain at 10×10 km to the nested domain at 5×5 km. Instead, run fixBC used idealized default boundary profiles of ozone obtained from the NOAA-Aeronomy Laboratory Regional Oxidation Model (NALROM). These profiles are climatological and based upon northern hemispheric, mid-latitude, clean environment conditions. By comparing fixBC with BASE, the importance of ozone import to the UK during the heatwave events could be investigated.

2.5 Performance metrics

The evaluate WRF-Chem's performance in simulating observed ozone during Summer 2019 we have used a range of established metrics. These are: normalised mean bias (NMB, Eq.1), root mean square difference (RMSD, Eq.2), index of agreement (IOA, Eq.3), Pearson's Coefficient (R, Eq.4), mean fractional bias (MFB, Eq.5) and mean fractional error (MFE, Eq.6):

$$\mathrm{NMB} = \frac{\sum_{i=1}^{n}(M_i - O_i)}{\sum_{i=1}^{n}(O_i)} \quad \text{(Eq.1)}$$

$$\mathrm{RMSD} = \sqrt{\frac{\sum_{i=1}^{n}(M_i - O_i)^2}{n}} \quad \text{(Eq.2)}$$

$$\mathrm{IOA} = 1 - \left[\frac{\sum_{i=1}^{n}(O-M)^2}{\sum_{i=1}^{n}(|M-\bar{O}|+|O-\bar{O}|)^2}\right] \quad \text{(Eq.3)}$$

$$\mathrm{R} = \frac{n(\sum_{i=1}^{n} M_i O_i) - (\sum_{i=1}^{n} M_i)(\sum_{i=1}^{n} O_i)}{\sqrt{[n\sum_{i=1}^{n} M_i^2 - (\sum_{i=1}^{n} M_i)^2][n\sum_{i=1}^{n} O_i^2 - (\sum_{i=1}^{n} O_i)^2]}} \quad \text{(Eq.4)}$$

$$\mathrm{MFB} = \left(\frac{1}{\mathrm{n}} \sum_{\mathrm{i}=1}^{\mathrm{n}} (\mathrm{M_i} - \mathrm{O_i})/((\mathrm{O_i} + \mathrm{M_i})/2)\right) \times 100 \quad \text{(Eq. 5)}$$

$$\mathrm{MFE} = \left(\frac{1}{\mathrm{n}} \sum_{\mathrm{i}=1}^{\mathrm{n}} |\mathrm{M_i} - \mathrm{O_i}|/((\mathrm{O_i} + \mathrm{M_i})/2)\right) \times 100 \quad \text{(Eq. 6)}$$

NMB, RMSD, IOA and R are metrics that are widely adopted in the air quality literature to evaluate models (e.g., Huang (2025) [82]). The MFB and MFE metrics were proposed by Boylan and Russell (2006) [83] and are also recommended as best practice for operational evaluation of CTMs [84]. MFB and MFE are expressed in two different range of values: "goal" values in which the performance of the model in reproducing the correct magnitude of concentrations can be considered good and the "criteria" values for which the performance of the model can be considered average. Values of MFB and MFE outside the "goal" and "criteria" ranges highlight a poor representation of concentrations and indicate unreliable model performance. The "goal" range is set at MFE ≤ 50% and MFB ≤ ±30% while the "criteria" range is set at MFE ≤ 75% and MFB ≤ ±60%. Values of MFE > 75% and -60% > MFB > 60% are representative of poor model performance.

3. Model Evaluation

In this section, we evaluate the performance of the WRF-Chem BASE run in reproducing observed ozone and temperature during the full Summer 2019 period. Hourly observations of ozone (AURN) and T_{2m} (MIDAS), separated by urban and rural backgrounds stations, are compared to hourly model outputs in **Figure S1**. For these comparisons, the model outputs were sampled at the closest latitude and longitude of the observations. Note, AURN and MIDAS data are measurements taken at a particular geographical point, while WRF-Chem outputs are representative of an average quantity within a grid square of 5×5 km spatial resolution. This difference should be borne in mind while interpreting model biases. The model performance has been analysed using a range of metrics (Sect.

2.5; MNB, RMSD, IOA, R, MFB, MFE) which are reported in **Table 2** (urban background sites) and **Table 3** (rural background sites) for June, July and August individually and as an average for the whole summer of 2019.

Table 2: Statistical evaluation of WRF-Chem's performance in reproducing observed surface ozone and T_{2m} at urban background sites from the AURN and MIDAS networks. The various metrics (NMB, RMSD, IOA, R, MFB, MFE; see main text) were calculated for individual sites and then averaged over all sites for June, July and August and for the full summer period (JJA) of 2019. The units of RMSD are μg/m^3 or °C, NMB, MFB and MFE are expressed in % and IOA and R are unitless. Results are shown for the BASE model run.

Metric	June 2019		July 2019		August 2019		JJA Average	
	O_3	T_{2m}	O_3	T_{2m}	O_3	T_{2m}	O_3	T_{2m}
NMB (%)	-4.12	8.48	-5.81	2.18	-9.10	-8.35	-6.50	-1.36
RMSD	12.26	1.85	13.25	1.58	13.06	2.18	12.85	1.87
IOA	0.80	0.93	0.83	0.94	0.86	0.88	0.84	0.92
R	0.68	0.92	0.71	0.90	0.77	0.86	0.74	0.86
MFB (%)	-6.80	8.01	-8.14	2.22	-11.05	-9.68	-8.99	-1.66
MFE (%)	20.71	10.27	25.90	7.95	23.43	12.94	23.47	10.41

Table 3. As Table 2 but for rural background sites.

Metric	June 2019		July 2019		August 2019		JJA Average	
	O_3	T_{2m}	O_3	T_{2m}	O_3	T_{2m}	O_3	T_{2m}
NMB (%)	-19.46	4.29	-19.03	-1.42	-21.17	-14.57	-20.46	-6.49
RMSD	14.48	1.56	14.89	1.54	15.46	2.70	15.14	2.10
IOA	0.70	0.93	0.77	0.93	0.78	0.76	0.76	0.87
R	0.77	0.90	0.76	0.87	0.83	0.84	0.80	0.81
MFB (%)	-22.80	3.21	-21.32	-2.01	-24.15	-17.15	-23.62	-7.60
MFE (%)	23.89	9.83	24.37	9.18	25.60	18.7	25.37	13.54

WRF-Chem reproduces the observed hourly ozone concentrations well but exhibits a low bias (i.e. negative NMB) at both urban and rural sites. The observed ozone magnitude is better captured at urban locations where for each month the NMB is <10% and the IOA >0.8, while at rural sites the bias is larger (NMB up to ~ -20%). Similarly, averaged over the full summer period, the RMSD is lower at urban (~13 μg/m^3) compared to rural (~15 μg/m^3) sites. The Pearson coefficients (R), a measure of how observed and modelled ozone co-vary, are 0.74 (urban) and 0.8 (rural) over the full summer period. This shows that the hourly variations in ozone are generally well captured by the model.

For temperature, the magnitude of observed T_{2m} is reasonably well reproduced in the months of June and July (NMB range from -1.4% to +8.5% across site types), though a more significant cold bias (NMB range of -8.3 to -14.6 %) is apparent for August. The cold bias in modelled T_{2m} may be explained by spatial resolution. Each model grid cell has an area of 25 km^2, while the point observations from MIDAS are representative of more local conditions that are not always captured by CTMs even when run at this fairly high resolution. Over the full summer period, correlation coefficients are found to be slightly higher in urban areas (R = 0.86) than in rural areas (R = 0.81) and the overall IOA between model and observation is similar across site types (~0.9). This demonstrates that observed hourly T_{2m} variations are well reproduced over this period.

To further evaluate the WRF-Chem simulation, we add to the classic statistical metrics the mean fractional bias (MFB) and error (MFE) following the method presented by Boylan and Russell (2006) [83]. Recall from Section 2.5, "goal" (MFB ≤ ±30%; MFE ≤ 50%,) and "criteria" (MFB ≤ ±60%; MFE ≤ 75%) levels are used in the interpretation of these metrics. Within the "goal" range, model performance can be considered good (i.e. low bias), while within the "criteria" range model

performance can be considered acceptable. Outside of the "goal" and "criteria" ranges indicates poor performance and unreliable model outputs. For both MFB and MFE, modelled ozone and T_{2m} were within the "goal" range for individual months and at both urban and rural sites (**Table 2, 3**).

4. Results and Discussion

4.1 Ozone and temperature enhancements during heatwaves

In Section 3, we showed that the model BASE run reproduces hourly ozone and T_{2m} observations well over the summer 2019 period. We next examine enhancements of ozone and T_{2m} that occurred during the three heatwave periods. **Figure 2** shows observed and modelled daily maximum 8-hour running mean ozone concentration (MDA8) and daily maximum T_{2m}. These time series cover the full summer period and data are averaged across all AURN site locations. MDA8 is a common metric used to inform exposure and epidemiological studies on human health [85] that is incorporated into UK air quality regulations. Enhancements of MDA8 ozone during each heatwave event is clearly apparent, and the observed-modelled correlation (R=0.9) shows that mean MDA8 variations over the full summer period are very well captured by the model. Both the AURN measurements and model show that site-averaged MDA8 ozone exceeded a concentration of 100 μg/m^3 in each heatwave period (**Figure 2a**), while at all other times it was below this threshold. A concentration of 100 μg/m^3 is significant as it marks the boundary between 'low' and 'moderate' health risk in the UK's air quality index [86] which is informed by health studies (e.g., [87]). Reproducing extreme events is generally very challenging for process-based air quality models [28, 88, 89]. However, **Figure 2a** shows clearly that WRF-Chem reproduces the peak MDA8 ozone enhancements during the heatwave periods well. The observed maximum MDA8 values occur on June 27th, July 25th and August 25th and are reproduced by the model to within roughly ± 5 μg/m^3.

To explore spatial variability in the sign and magnitude of the heatwave-associated ozone and T_{2m} responses, anomalies of both variables are shown in **Figure 3.** This analysis is presented separately for the June/July/August heatwave events. Here, the anomalies represent the percentage difference in hourly ozone or T_{2m} during all of the heatwave (HW) periods in each month relative to all of the non-heatwave periods (non-HW) in the same month. From this analysis, it is evident that the ozone response differed considerably both spatially across the UK and across the three HWs. For each event, there were both positive and negative ozone anomalies in some parts of the UK. This was particularly clear during the July HW when the observations showed a distinct West–East gradient; negative ozone anomalies in western regions (England and Wales) and strong positive anomalies in the East of England – a pattern well reproduced by the model (**Figure 3b**). For the June and August events, the model produces a smoother, more evenly distributed anomaly field compared to that observed, missing some of the finer scale local variations seen at individual monitoring stations. This is consistent with the relatively coarse 5×5 km spatial resolution used in the simulations that will not resolve the most local effects. According to both the observations and model, ozone enhancements were most widespread and strongest during the August HW, reaching up to ~63% in the South-East of England (**Figure 3c**). The scatterplot in **Figure S2** shows the correlation between the hourly observed and modelled anomalies of ozone and T_{2m} during the three individual HW events in June, July and August. The correlation between model and observations is high during all three periods with R between 0.83 and 0.9 for ozone anomalies and between 0.89 and 0.94 for temperature anomalies.

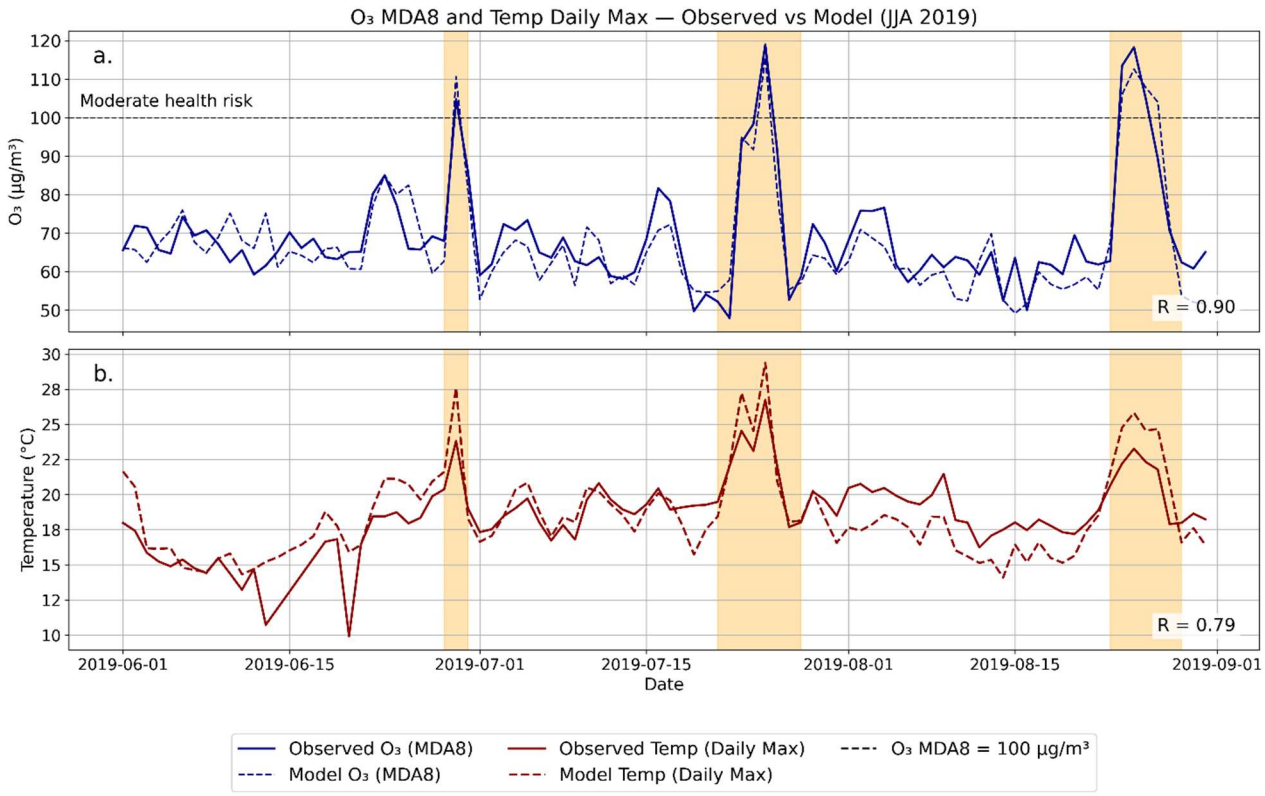

Figure 2. Observed and modelled (a) MDA8 O_3 (µg/m^3) and (b) 2-m temperature (°C) over summer 2019 averaged over all AURN site locations. The orange shaded regions denote 'heatwave' periods. The ozone concentration threshold of 100 µg/m^3 is annotated with a dashed horizonal line. R values (model-measurement correlation coefficient) are annotated. Model results are from the WRF-Chem BASE run.

For daily maximum temperature, the model captures the site-averaged variations (R=0.79) of the measurements reasonably well over the full summer period (**Figure 2b**). However, on average, the model overpredicts the peak temperatures during all three HW events by up to several °C. In terms of spatial variations, anomalies were consistently positive during all three HWs and were generally well captured by the model, particularly in June and July (**Figure 3d, e**). In August, the model tended to overestimate the anomalies compared with observations (**Figure 3f)**. Our analysis suggests that this may be linked to very dry soil moisture conditions simulated by the model, with anomalies up to 40% during the HW days of this month compared to the non-HW days (**Figure S3**). Reduced soil moisture may limit evaporation, enhance sensible heat flux, and amplify temperature anomalies – a feedback mechanism that has been highlighted in previous studies of European HWs [90].

The observed and modelled ozone-temperature relationship obtained from all hourly data in all three HW periods is shown in **Figure 4a**. A linear regression reveals a moderately strong positive relationship between the two variables in both the observed (R^2 =0.7) and modelled (R^2 =0.8) datasets. A positive ozone-temperature relationship is consistent with findings from previous studies both in the UK [21] and in other parts of Europe and elsewhere [14, 91]. The slopes of the regression lines for both the observed and modelled datasets in **Figure 4a**, often referred to as a "climate penalty factor" (CPF), are in close agreement: 5.9 µg/m^3 °C^{-1} (observations) and 5.5 µg/m^3 °C^{-1} (model; run BASE).The same quantities calculated for all non-HW periods (not shown) over summer 2019 were: 2.2 µg/m^3 °C^{-1} (observations) and 3.8 µg/m^3 °C^{-1} (model; run BASE), suggesting a stronger ozone-temperature sensitivity during HW periods. An alternative approach to estimate the CPF during the HW periods is also shown in **Figure 4b-e** that follows the method of Bloomer (2009) [13]. In this analysis, hourly ozone was separated by 10 temperature bins, and the ozone-temperature relationship is expressed for different percentiles of the ozone distribution. This analysis demonstrates the positive ozone-temperature association *across* the ozone distribution and shows that the sensitivity is stronger at higher percentiles. For example, from the observed data: 5.24 µg/m^3 °C^{-1} at the 25th percentile versus 6.49 µg/m^3 °C^{-1} at the 95th percentile. The model also shows

a stronger ozone-temperature sensitivity for the 95th percentile (5.67 μg/m^3 °C^{-1} in the BASE run), though it is lower than that observed by ~14%.

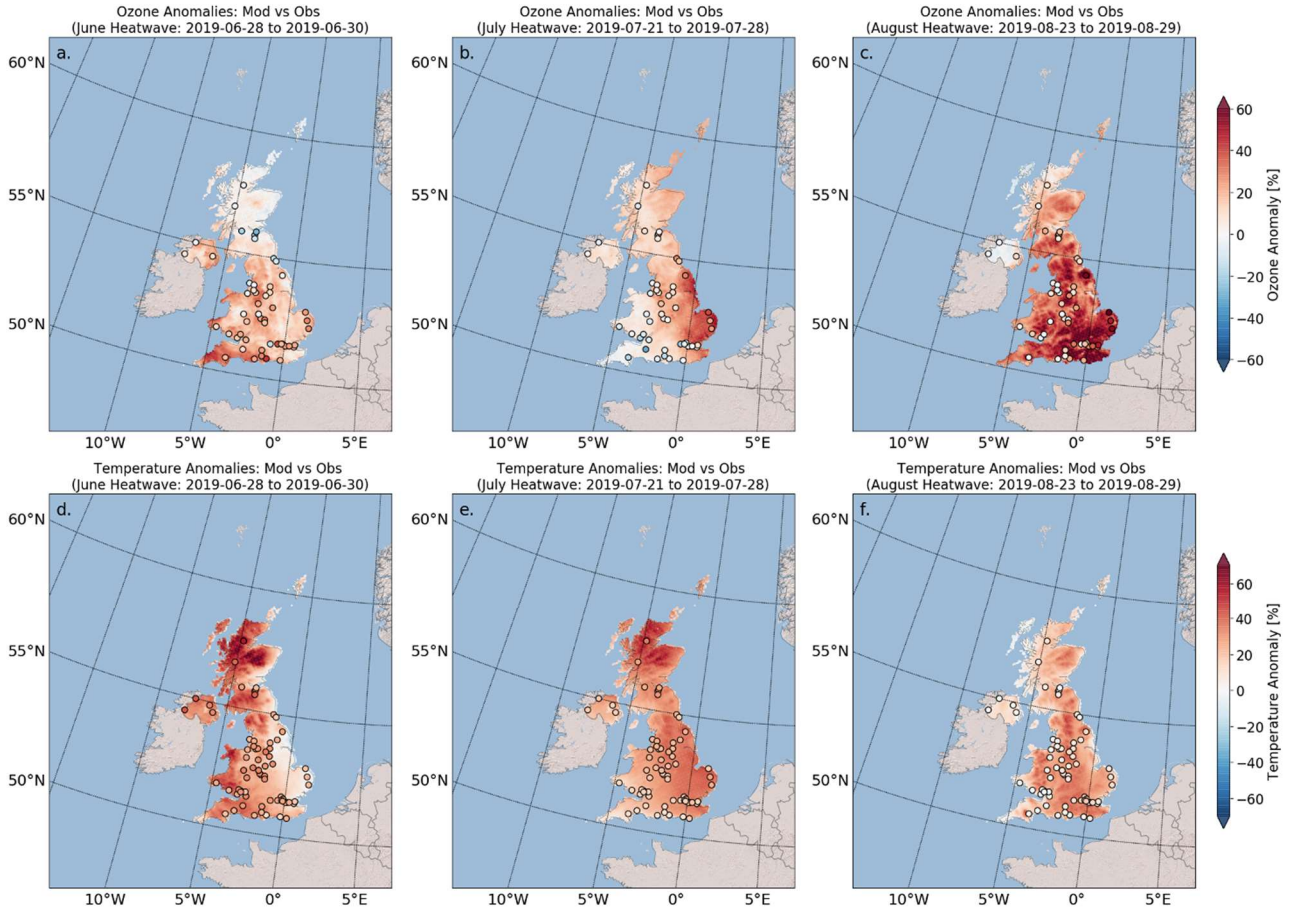

Figure 3. Anomalies (%) of hourly (a-c) ozone and (d-f) 2-m temperature, for June, July and August 2019. Anomalies represent the difference between ozone (hourly) averaged over the HW and non-HW periods of a given month. Filled circular points show observed anomalies. Background contours show results from the WRF-Chem BASE run.

In summary, the analysis in this section demonstrates that ozone concentrations across much of the UK were markedly larger during the three HW periods of summer 2019 relative to non-HW periods. WRF-Chem captures the variability of ozone well over this period, including the mean enhancements of MDA8 ozone above 100 μg/m^3, as well as the ozone-temperature response. This lends confidence to the usefulness of WRF-Chem as a tool to investigate the drivers of the ozone enhancements in the ensuring discussion.

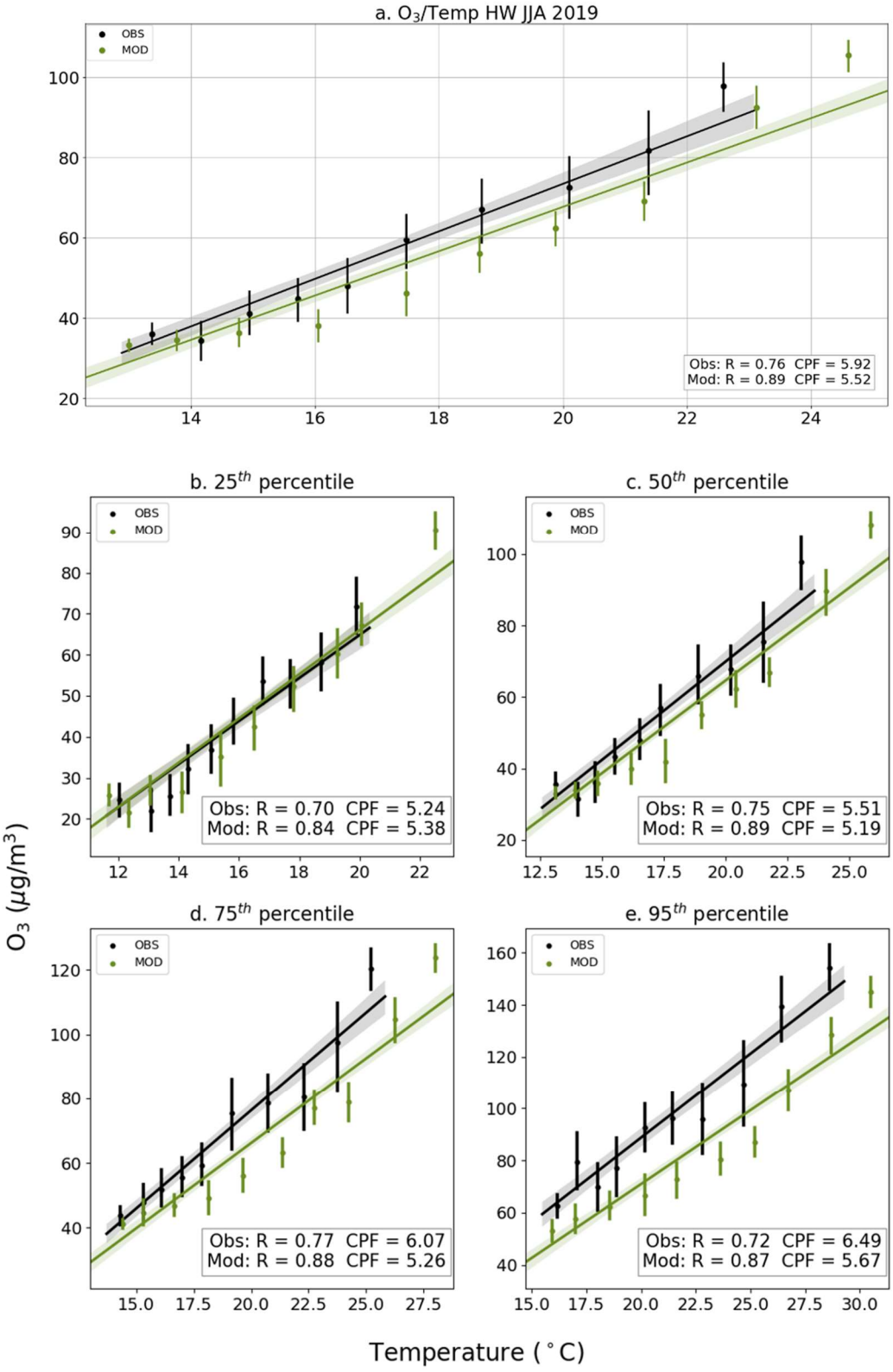

Figure 4. Observed and modelled ozone-temperature relationship during HW periods. The relationship is based on hourly data at AURN site locations over HW periods only. Panel (a) shows the relationship for the full ozone and temperature distribution. Panels (b-e) show the relationship for different percentiles of the ozone distribution (see main text). The slopes of linear regression lines, referred to as the 'climate penalty factor' (CPF; $\mu g/m^3\ °C^{-1}$), are annotated in each panel. R^2 values are also annotated to illustrate the goodness of fit of the linear model. Model results are from the WRF-Chem BASE run.

4.2 Ozone budget

In this section we analyse the chemical and physical drivers of ozone concentration enhancements during the HW periods. The modelled net chemical ozone production rate (obtained from the chemical tendency variable *chem_o3; see Sect. 2.3.3*) is shown in **Figure 5** for the surface level of the 5×5 km UK domain. These maps show the average chemical ozone tendency during the 'midday' period (from 11am to 3pm) for all HW (**Figure 5a**) and for all non-HW periods (**Figure 5b**) and as difference between HW and non-HW period (**Figure 5c**). Outside of the HWs, our budget analysis indicates a net positive rate of midday ozone production across a great part of the UK, with typical values of around 1-5 ppb/hr. Qualitatively, this is consistent with the previous work of Coyle (2003) [92] who estimated a net positive rate of ozone production in summertime. During the HW periods, net chemical ozone production is clearly enhanced and shows significant spatial variability. In the South-West and South-East of the England, rates of up to ~ 8.20 ppb/hr are seen which correspond to relative enhancements above the non-HW periods of up to + 4.2 ppb/hr. Central England rates increased up to ~ 6.9 ppb/hr (+ 3.4 ppb/hr) while the North of England and Scotland see smaller absolute rates ~ 5 ppb/hr, though enhancements in HW periods relative to non-HW periods are still relatively large; corresponding to + 2.7 ppb/hr (**Figure 5c**). The ozone chemical tendencies are found to be negative in the major urban areas of the UK where processes of ozone destruction (e.g., NO_X titration) seem to be predominant both in the HW and non-HW periods. The full diurnal cycle of net chemical ozone production, averaged across the entirety of the UK, is shown in **Figure S4**. This highlights how on average the peak ozone production rate (at ~ 12pm) approximately doubles between non-HW and HW periods.

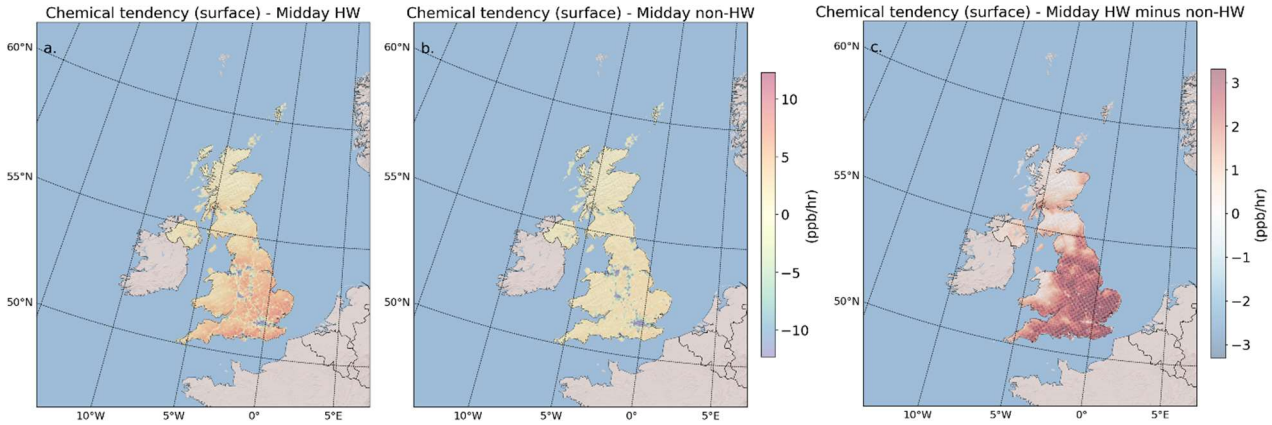

Figure 5. Net chemical tendency of ozone (ppb/hr) at the surface level (max height 20m a.g.l.) diagnosed by WRF-Chem (BASE run). The net production is shown averaged for the midday period between 11am and 3pm and for (a) all of the HW periods, (b) all of the non-HW periods of summer 2019 and (c) the difference between the two periods.

Alongside chemical production and loss, it is well established that ozone concentrations are strongly impacted by dry deposition [17, 92]. Dry deposition rates of ozone depend on both the near-surface ozone concentration and the deposition velocity. The latter is affected by a range of factors, including surface type and meteorological conditions (e.g. wind speed) that affect resistance to atmosphere-surface exchange. In their case study of UK ozone during the 2003 HW, Vieno (2010) [17] considered the effects of dry deposition on surface concentrations through a sensitivity analysis. Removing the process of ozone dry deposition entirely from their model, Vieno (2010) [17] found, as expected, ozone increases on most HW days (increases of around ~ 20-35 ppb), though with significant temporal variability.

Our analysis shows that the ozone dry deposition rates increased across the entirety of the UK during HW periods relative to non-HW periods (**Figure 6a-c**). This reflects increased ozone availability and occurred in spite of decreases in deposition velocity (**Figure 6d-f**) simulated across much of the UK. Additionally, dry deposition was analysed across land-use types during HW and non-HW conditions using a fractional land-use weighting approach (**Figure S5**). High-resolution (1×1 km) UKCEH Land Cover 2019 data [93] were resampled to the model grid (5×5 km), retaining both the dominant land-use class and the fractional coverage of each land-use type within each grid cell to preserve sub-

grid heterogeneity and allowing a more representative quantification of deposition over mixed land use categories. Individual land-cover classes were grouped into broader categories, including woodland, arable, grasslands, freshwater, marine environments, and urban areas. Mean dry deposition fields for HW and non-HW conditions were then attributed to each land-use group using weighted contributions based on sub-grid land-use fractions, rather than assuming a single dominant land-use per model cell. Distributions of dry deposition for each land-use group were compared between HW and non-HW. Higher median deposition was found during HW both in natural (e.g., arable, grassland ~0.020 g m^{-2}) and urban areas of UK (up to ~0.010 g m^{-2}). Highest variability was observed in arable (up to ~0.038 g m^{-2}) and grassland (up to ~0.036 g m^{-2}) areas. Land use categories showing similar median deposition between HW and non-HW periods were woodlands (~0.09 g m^{-2}) and semi-natural grasslands (~0.012 g m^{-2}) while categories where the median deposition was higher during non-HW periods were heathlands (~0.012 g m^{-2}) and freshwater, rocks (~0.010 g m^{-2}).

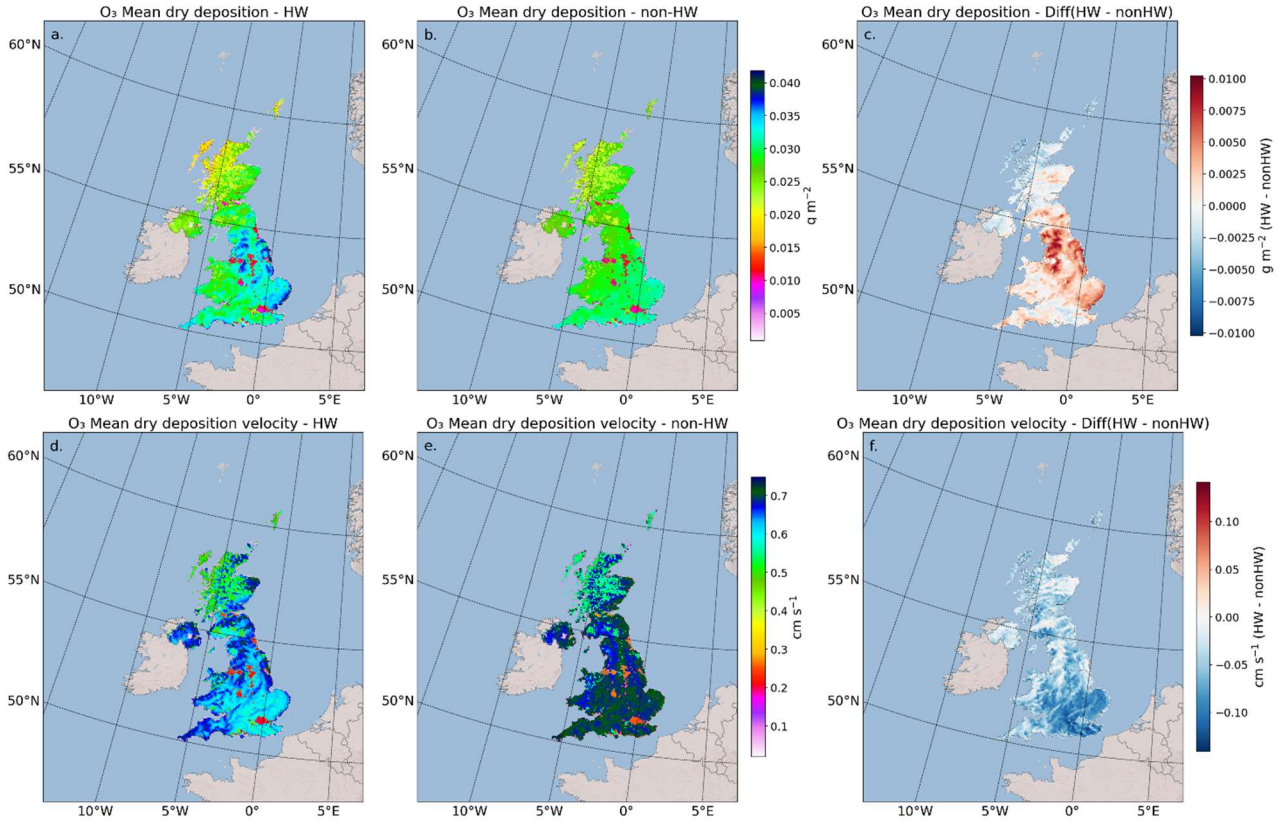

Figure 6. Modelled mean (a-b) dry deposition rate (g/m^2) and (d-e) deposition velocity (d-f; cm/s) during HW and non-HW periods of summer 2019, including (c-d) the absolute difference between the two (HW minus no-HW; right-hand column).

To construct a spatially integrated budget, the net chemical ozone production and transport tendency terms (e.g., advection) have been integrated over the entire UK domain for each vertical level included in the model setup below the boundary layer (**Figure 7**). Ozone concentrations are found between 20 and 30 ppb/hr during the non-HW period as an average over all of the UK with positive gradients going from ground level to 1 km of height (**Figure 7a**). During the HW periods ozone concentrations increase above 50 ppb/hr on average over the whole UK domain and throughout the boundary layer (**Figure 7a**, within the red dashed brackets). The increase in ozone levels during the HW periods – as modelled by WRF-Chem – is linked to concurrent factors. First, the horizontal and vertical advection is described as positive (ozone enriched air entering into the domain) for the majority of the days both during the HW and the non-HW periods (**Figure7b**). This phenomenon is limited to the altitudes below the planet boundary layer height (black dashed line in **Figure 7**), while above the advection term is predominately negative (ozone enriched air exiting from the domain). Second, the vertical mixing appears to be always negative below the planet boundary layer height (**Figure 7c**) suggesting that ozone produced at surface level is trapped below the boundary layer, while above it the values are zero or slightly positive. Third, the net chemical production of ozone is

in mostly positive during the whole summer period (as average of the whole UK area), though peaks of production below and above the boundary layer occur during the HW periods (**Figure7d**). Finally, the presence of convective system episodes (**Figure7e**) enhances the production of ozone in particular during the first 20 days of June when thunderstorms and heavy rain occurred with several weather warnings issued by the Met Office (see Section 2.1.1).

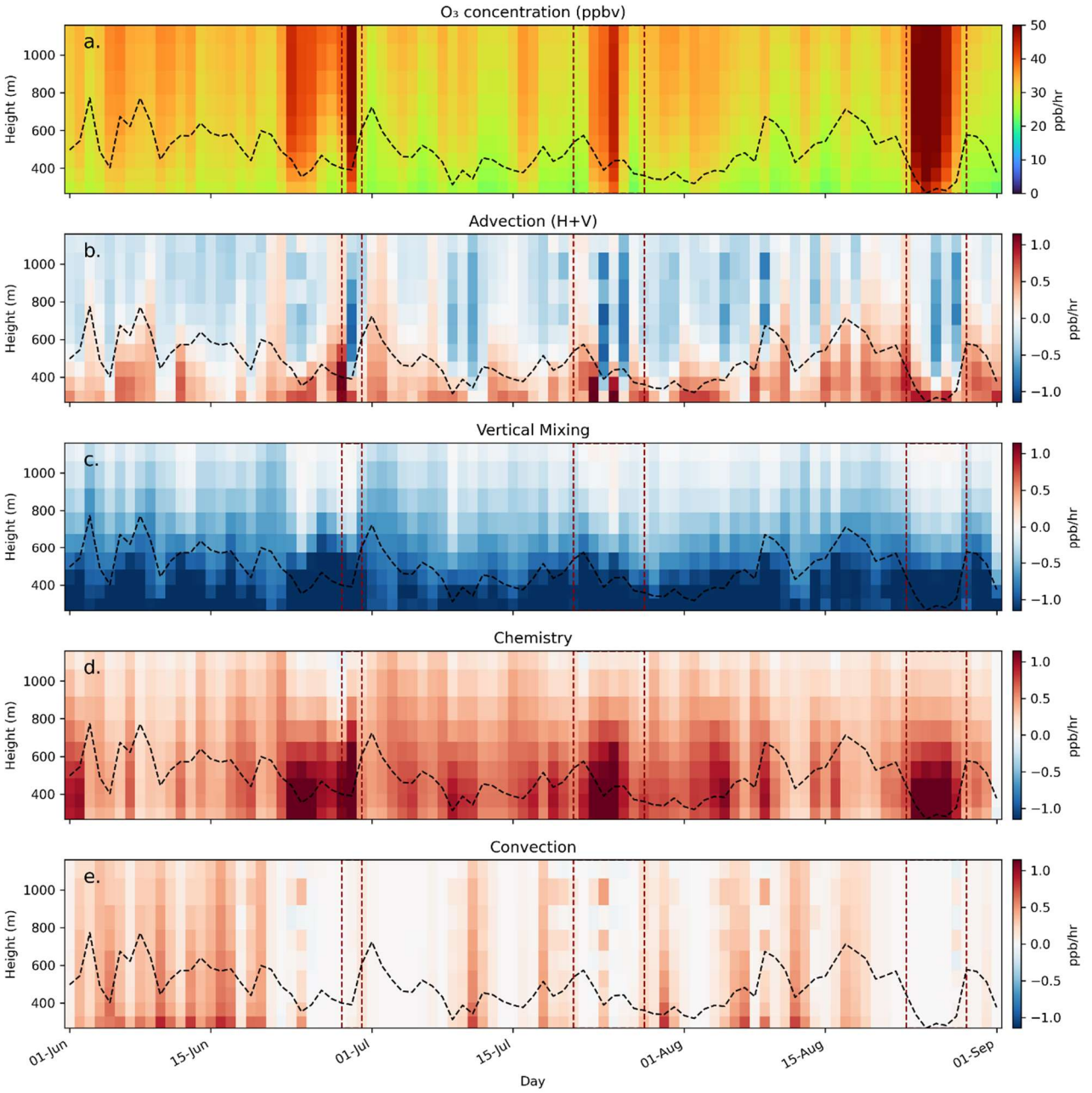

Figure 7. Time series of daily averaged ozone concentration (a) and tendencies in ppb/hr obtained from the WRF-Chem diagnostic variables of horizontal and vertical advection (b), vertical mixing (c), net chemical production (d) and convection (e) for the whole domain of UK and for the full summer period 2019. The dashed brackets highlight the period of HW for the three months, while the black dashed line highlight the daily variation over the planetary boundary layer height. The y-axis shows the first 1 km of height a.g.l. of model output concentrations.

There are few quantitative assessments of the UK ozone budget with which to compare our findings. However, a simple budget analysis was performed by Coyle (2003) [92] for the winter and summer of 1996 using ozone observations from various monitoring sites and a simple box model of the UK boundary layer, including a simple estimate of deposition. The analysis by Coyle (2003) [92] suggested that the UK was a net sink for ozone for the majority of the year, but a net source in summer months. Over their summertime period (May-August) a mean rate of net chemical ozone

production of 180 Mg/hr (132 Gg/month) for the UK was obtained with ozone loss from deposition being -237 Mg/hr (-173 Gg/month). Our results for Summer 2019 indicate net chemical production rates of 119, 153 and 120 Gg/month and the dry deposition of -216, -179 and -182 Gg/month for June, July and August, respectively. Qualitatively, our results are similar in that they show net chemical ozone production is positive during the summer period and that net chemical production less deposition is negative. Quantitative differences from the calculation done by Coyle (2003) [92] can be expected given interannual variability and also a 20 year difference between the analysis years. As well, there are notable differences in approach, with the earlier study based on measurements (albeit at a limited number of sites) and a simple box model versus a more sophisticated CTM approach here that accounts for regional differences in the physical and chemical processes on the individual budget terms.

4.3 Role of biogenic emissions

Isoprene is a biogenic VOC that plays an important role in photochemical ozone production. It is emitted from terrestrial vegetation and accounts for around half of global BVOC emissions [64]. Isoprene emissions are influenced by multiple factors, including light conditions and temperature [94, 95]. Extreme weather events such as HWs [31, 96] and droughts [16, 97] can significantly alter isoprene emissions, either increasing or reducing them. Modelling biogenic isoprene emissions online is therefore important for capturing the temperature-emissions response and for assessing its importance for ozone during HWs. Recall, in this study the MEGAN model, coupled online with WRF-Chem, calculates BVOC emissions using vegetation-specific activity factors and their responses to changes in temperature [64, 95].

There are very few datasets of UK-wide isoprene emissions with which to evaluate the emissions calculated from MEGAN in WRF-Chem. However, a top-down estimate of isoprene emissions for the year 2019 is available from an inversion of the MAGRITTEv1.1 CTM constrained by TROPOMI formaldehyde (HCHO) vertical columns [98]. This top-down emission estimate was produced on a 0.5°×0.5° grid and with weekly temporal resolution. The emissions were interpolated to the WRF-Chem 5×5 km grid using bilinear interpolation and monthly averaged isoprene emissions for June, July, and August are compared to those from our MEGAN/WRF-Chem simulation in **Figure S6**. Both the top-down and bottom-up (MEGAN) emission estimates carry significant uncertainty, and care should be taken in comparing them. The spatial distribution of the MEGAN emissions showed the best agreement with the top-down estimate in July, although the emissions in central England are larger than those in TROPOMI. In June, the TROPOMI-based product indicated higher emissions in northern UK and Northern Ireland, which were not reproduced by MEGAN, while central and southern England were in good agreement. In August, MEGAN tended to calculate larger emissions in comparison to TROPOMI, likely due to its sensitivity to temperature and soil moisture (**Figure S3, S6**). This overestimation in biogenic emissions appears to be linked to the model's overestimation of T_{2m} anomalies (**Figure 3**) and may have contributed to the corresponding overestimation of ozone anomalies (**Figure 3**).

Anomalies in biogenic isoprene emissions from WRF-Chem are shown for the three HW periods (**Figure 8a-c**). The model simulates a variable increase in emissions depending on the HW period. Correspondingly, isoprene concentrations at the surface are also enhanced. For the June HW, UK-wide isoprene emissions are estimated to have rose by ~109%, with an associated surface ozone concentration increase of ~13%; in July, isoprene emissions increased by ~81% with a 28% rise in ozone; and in August, a ~42% increase in isoprene corresponded to a much larger ozone increase of ~37% (**Table S2**). The magnitude of these simulated isoprene emission enhancements, along with the accompanying ozone increases, are of a similar order to that reported in other UK studies. For example, Ferracci (2020) [96] showed through field sampling that isoprene emissions increase up to 400% during HW periods. For the UK, a nonlinear relationship between isoprene concentration and ambient temperature was previously observed by Lee (2006) [27] during the HW of 2003. Their analysis, based on measurements from a site in London, showed high isoprene concentrations (along with other VOCs) and a shift in dominant sources from anthropogenic to biogenic, which increased the local O_3-formation potential. WRF-Chem captures a similar behaviour, with a strong correlation between isoprene and temperature (0.87 in urban areas and 0.82 in rural areas over the whole summer) (**Figure 8d, e**).

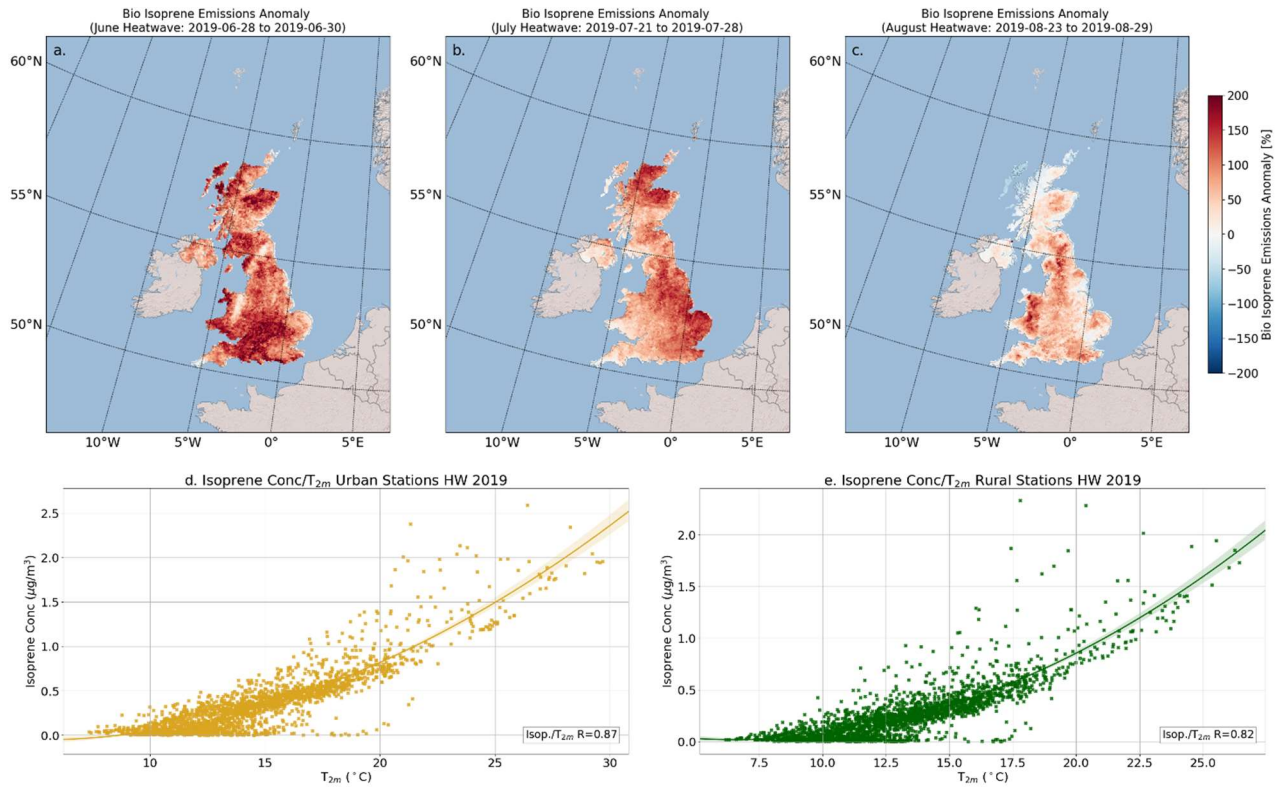

Figure 8. (a-c) Modelled biogenic isoprene emission anomalies (%) at the surface during the June, July, and August HWs of 2019. Anomalies are calculated as the difference in hourly isoprene biogenic emissions between HW and non-HW periods in each month. Panels (d) and (e) show the relationship between modelled hourly isoprene concentration and hourly 2-m temperature at urban and rural sites, respectively.

Local monitoring of isoprene itself would provide the most direct and strongest evidence for any HW-driven enhancements. However, measurements of surface VOC and BVOC concentrations in the UK are very limited and there are few data in 2019. In the absence of direct BVOC measurements, formaldehyde (HCHO) – an oxidation product of most VOCs, including isoprene – serves as a useful proxy for VOC emissions [99, 100]. Our analysis shows strong HCHO enhancements in the model during all three HW periods relative to non-HW conditions (**Figure 9**). The August HW in particular saw HCHO enhancements exceeding 200% across much of the UK. The magnitude and spatial distribution of these enhancements agree reasonably well with HCHO measurements from TROPOMI [98] over the same period and provides evidence for HW-induced BVOC emissions.

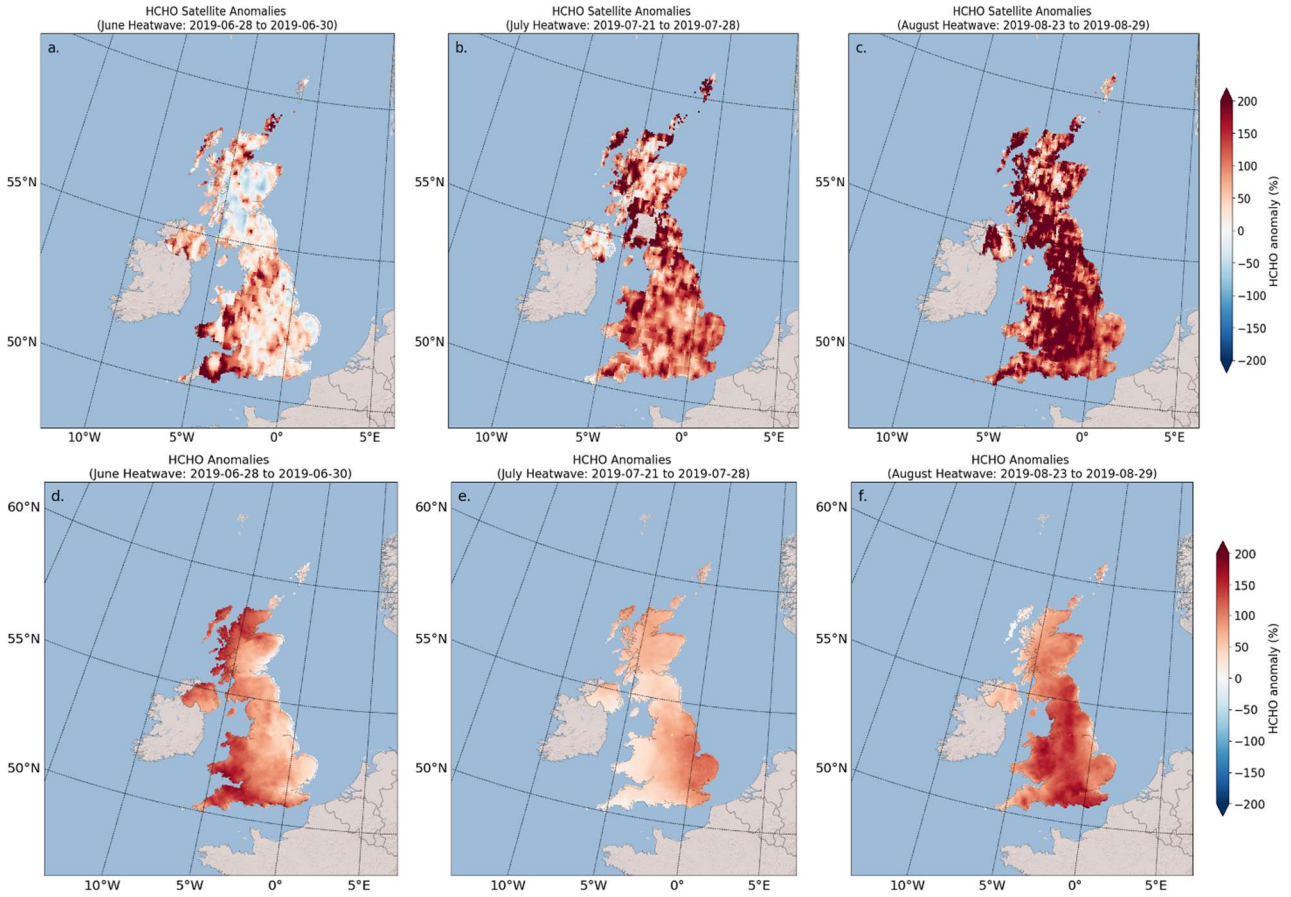

Figure 9. Anomalies in HCHO surface concentrations calculated between HW and non-HW periods of June, July and August 2019 from (a-c) TROPOMI satellite data at surface [98], and (d-f) WRF-Chem model output (BASE run).

4.4 Meteorological factors and import of ozone to the UK

It is well established that synoptic weather patterns may exert a strong influence on the surface concentration of air pollutants. High pressure systems, characterised by low wind speeds and temperature inversions, may limit pollutant dispersion and have been associated with elevated ozone concentrations in the UK [30] and many other world regions [101]. To explore the effect of air stagnation on ozone during the UK HWs of summer 2019, we calculated the hourly ventilation index (VI; m^2/s) from WRF-Chem outputs using Equation 7.

$$VI = WS \times PBL \qquad \text{(Eq.7)}$$

The VI metric is expressed as the product of wind speed (WS; m/s) and planetary boundary layer (PBL; m) height. It has been adopted in previous work to quantify the potential for smoke or other air pollutants to disperse from a source [102], quantify the impact of local sources of air contamination against regional transport phenomena [103] and to evaluate the health effects of air pollution exposure [104]. Here we use the VI metric to highlight particular conditions that contribute to enhanced levels of ozone during the August HW. **Figure 10** shows a time series of hourly modelled concentrations of NO_2 and ozone and VI metric for the period 20th to the 31st of August, highlighting the HW period between the 23rd and the 29th. Inspecting the night-time periods within the HW, it is evident that the ventilation index is at its weakest (always below ~ 100 m^2/s). The poor air circulation over night-time enhances the accumulation of ozone precursors (e.g., NO_2, blue line in **Figure 10**) that will contribute to spike up the concentrations of ozone during the following day. This kind of phenomenon has been already observed in the case of Los Angeles [105]. The VI was ~ 100 - 300 m^2/s during the HW period nights but increased up to ~ 700 m^2/s during nights from the 30th of August allowing polluted air to be flushed out from the boundary layer and reduce the air contamination.

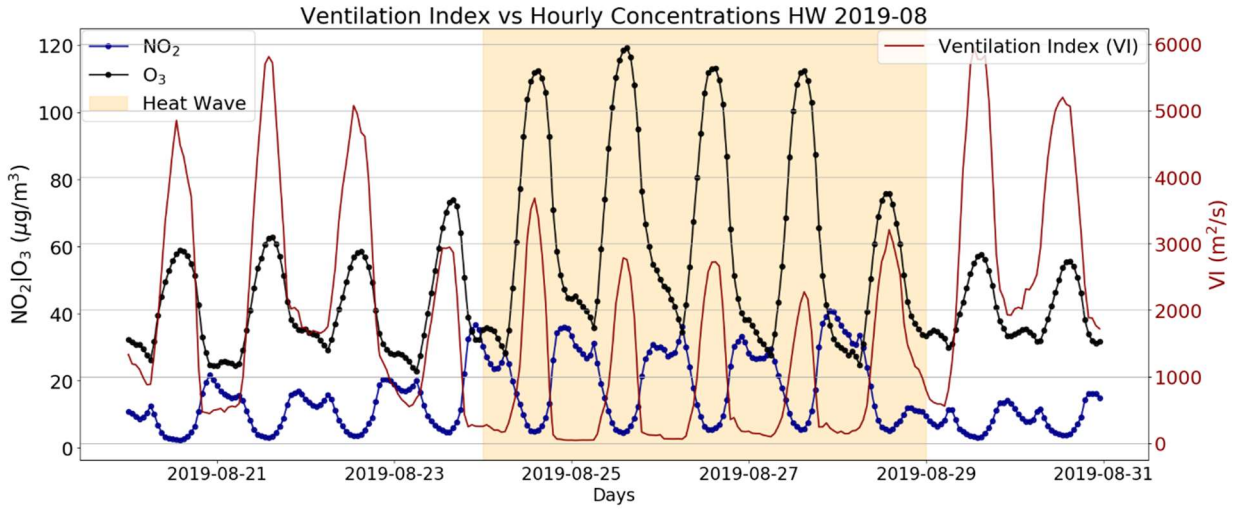

Figure 10. Hourly time series of modelled surface ozone (black line), NO_2 (grey line) and the Ventilation Index (VI; see main text) for the period of 20th August to 30th August 2019 including the HW from the 24th to the 29th. Average hourly values of these variables were calculated over all urban and rural background locations. Concentrations are expressed in μg/m^3, VI in m^2/s.

Alongside air stagnation, another important influence on the surface concentration of ozone at a given location is advection [106]. For the UK, surface ozone concentrations are determined not only by local (i.e. within UK) chemical production, loss and deposition, but also strongly by the import of ozone and its precursors from outside of the UK. This is addition to the presence of a wider hemispheric baseline ozone abundance [23]. Most recently, Romero-Alvarez (2022) [107] performed a detailed ozone source attribution study for the UK using a "tagging" approach implemented in WRF-Chem. Their results showed substantial differences in the relative importance of precursor emissions from different source regions on UK ozone, varying with the receptor region and seasonally. For example, the transport of continental European ozone to the UK by South-easterly winds was shown to contribute to summertime ozone pollution events in the eastern, southern, and South-West of the UK. Focussing on the 2003 HW, Vieno (2010) [17] also demonstrated that the import of ozone to the UK was a major influence on most days of this event, contributing tens of ppb throughout much of the UK domain, and even greater levels at sites in the South-East of England.

To explore the effect of air import to the UK during the 2019 HWs, a time series of observed and modelled site-averaged MDA8 ozone is shown in **Figure 11a** for both the BASE and fixBC runs. The difference between the two runs is shown in **Figure 11b**. This analysis shows that the import of ozone and/or its precursors to the UK over the three HW periods was a major contributor to MDA8 ozone over the UK. The difference between the two runs (fixBC minus BASE) reaches around ~ 26.6 μg/m^3 across the three events, with the import contribution raising local MDA8 to >100 μg/m^3 during each event. The effect of the import contribution is significantly larger than that of isoprene emissions as can be seen by comparing the ΔO_3 (fixBC minus BASE) with ΔO_3 (noISOP minus BASE) in **Figure 11b** with the latter reaching 11.6 μg/m^3 of maximum difference during HW periods.

To highlight spatial differences in the import contribution, the difference in MDA8 ozone between the runs fixBC and BASE is shown on a map in **Figure S7**, along with the modelled wind vectors. The import contribution is important across the whole of England, though is clearly largest over the South and South-East. During the HWs, southerly and South-easterly winds transported ozone and/or its precursors from continental Europe, where the effects of the summer HW were also felt to the UK [108-110]. Qualitatively, this is consistent with the findings of Vieno (2010) [17] in their case study of the 2003 UK HW.

An important conclusion by Romero-Alvarez (2022) [107] was that more stringent emission controls over continental Europe would be required to improve MDA8 over the UK (a metric relevant for human health). Our analysis in **Figure S8** corroborates this finding and leads to a similar conclusion. According to model data, the highest number of exceedances above 100 μg/m^3 by model grid per

day occurred during the three HW periods: 48, 88 and 168 during the HWs of June, July and August, respectively. During the non-HW periods only 9 and 1 exceedances by grid/day were modelled in June and July (**Figure S8a**). Of the total number of the MDA8 exceedances the fixBC scenario provided a reduction in the number exceedances relative to BASE of between 58 and 86%, while the noISOP scenario provided a reduction of around 30% (**Figure S8b**). These results help to contextualise the importance of long-range transport of polluted air (including ozone precursors) to the UK and underscore it as a major challenge for UK summertime air quality.

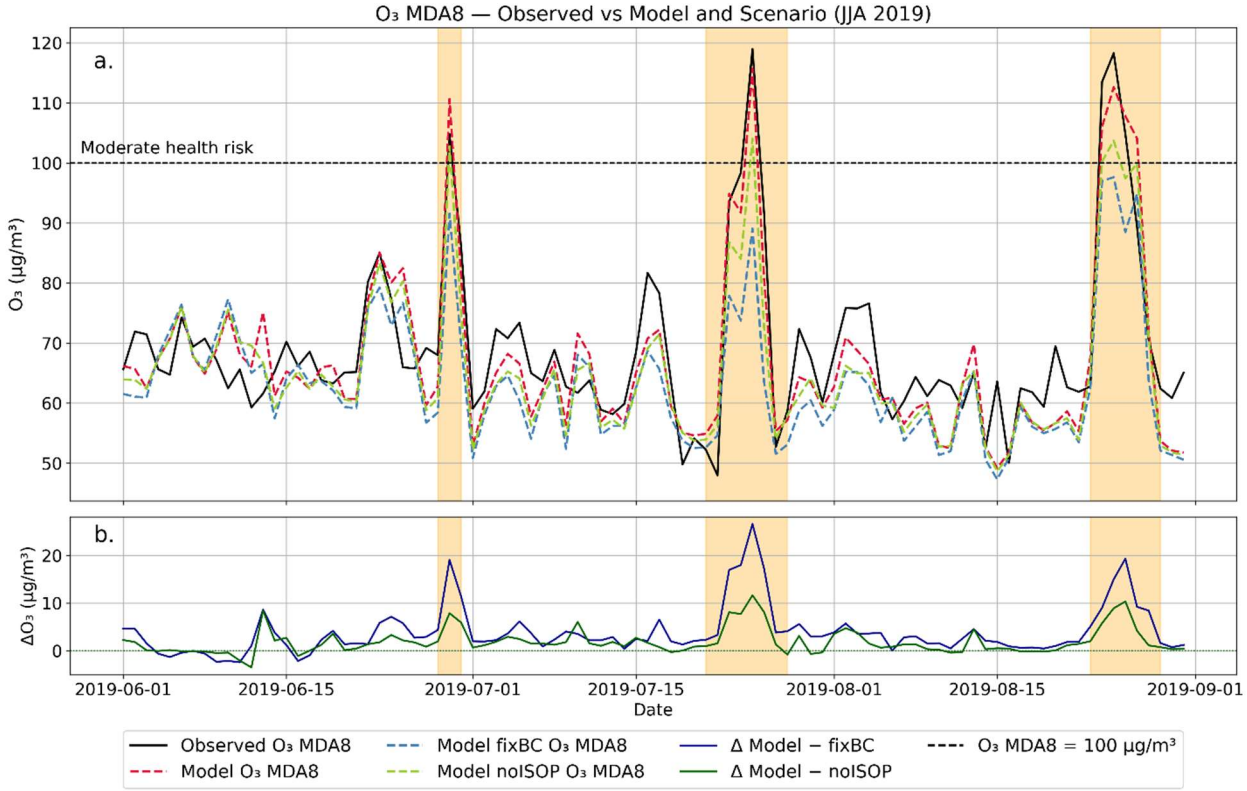

Figure 11. (a) Observed and modelled MDA8 ozone (µg/m^3) during summer 2019 averaged over all AURN site locations. Model data is shown for runs BASE, noISOP and fixBC. (b) Difference in MDA8 ozone between BASE run and sensitivity experiments (i.e. BASE minus noISOP; BASE minus fixBC). Shaded regions denote 'heatwave' periods. The ozone concentration threshold of 100 µg/m^3 is annotated with a horizonal line.

5. Summary and Concluding Remarks

We have used the WRF-Chem CTM to investigate the physical and chemical drivers of enhanced ozone levels observed over the UK during HWs in June, July and August 2019. The model is shown to reproduce ozone and temperature observations well over the full summer period, including the HW-associated ozone increases, and the ozone-temperature response. Our analysis reveals a marked increase in net chemical ozone production during each HW event, with parts of the UK seeing midday production rates of ozone up to +50% during the heatwave period of July. Based on online calculations using MEGAN, emissions of isoprene – a major biogenic VOC and important ozone precursor – increased substantially during the HW events. Although direct observations of isoprene during the HWs were unavailable, data from TROPOMI indicate large column HCHO enhancements (a VOC proxy) over much of the UK during the HWs (especially in August). These enhancements are well captured by the model. Meteorological conditions including weak wind speeds (i.e., low Ventilation Index) were found to contribute to air stagnation and the accumulation of ozone precursors during nighttime, with consequent enhanced ozone production during the following days. Ozone dry deposition was also significantly higher during HW periods and occurring in prevalence over natural areas calling for attention on the impact that it could have on vegetation. Despite enhanced local photochemical ozone production during the HW periods, a major contributor to ozone air pollution was the transport of air from outside the UK domain into the domain. This

transport of ozone (or ozone precursors) was responsible for elevating MDA8 above 100 μg/m^3, on average, during each of the three HW events. Our findings underscore the need for air quality mitigation policies to consider natural emissions, alongside reducing anthropogenic precursors, especially as HWs are expected to become more frequent and intense under a changing climate. Our results corroborate other modelling studies that have highlighted the prevalent role that long-range air transport has on UK summertime air quality. This highlights the necessity of concerted and continued European level efforts to tackle ozone air pollution.

Acknowledgements.

The present research has been supported by the National Environmental Research Council (NERC) grant Investigating HALocarbon impacts on the global Environment (InHALE) (NE/X003582/1). The authors declare that they have no known competing financial interests or personal relationships that could have appeared to influence the work reported in this paper. All simulations performed with WRF-Chem chemistry-transport model have been performed on the High End Computing (HEC) Cluster of the Lancaster University.

Authors contributions: Conceptualization – **RH AM**, Data curation – **AM**, Formal Analysis – **AM**, Funding Acquisition – **RH**, Investigation – **AM**, Methodology –**RH AM**, Visualisation – **AM**, Writing original draft – **AM**, Writing reviewing and Editing – **RH AM**.

Source data: NAEI emissions for UK used for all simulations are available from: https://naei.energysecurity.gov.uk/. CAMS regional emissions are available from: https://ads.atmosphere.copernicus.eu/datasets/cams-global-emission-inventories?tab=download. Fire emission inventory FINN is available from: https://www2.acom.ucar.edu/modeling/finn-fire-inventory-ncar . Initial and boundary conditions for meteorology are provided by NCAR: https://gdex.ucar.edu/datasets/d633000/ while chemical initial and boundary conditions are provided by CAM-Chem: https://www.acom.ucar.edu/cam-chem/cam-chem.shtml . The WRF-Chem model and all the preprocessors are downloadable from: https://www2.acom.ucar.edu/wrf-chem. Weather observations used for the model validation are available from: https://catalogue.ceda.ac.uk/uuid/dbd451271eb04662beade68da43546e1/. Hourly observations of air pollutants used for model validations are available from: https://uk-air.defra.gov.uk/networks/network-info?view=aurn.

Supporting Information

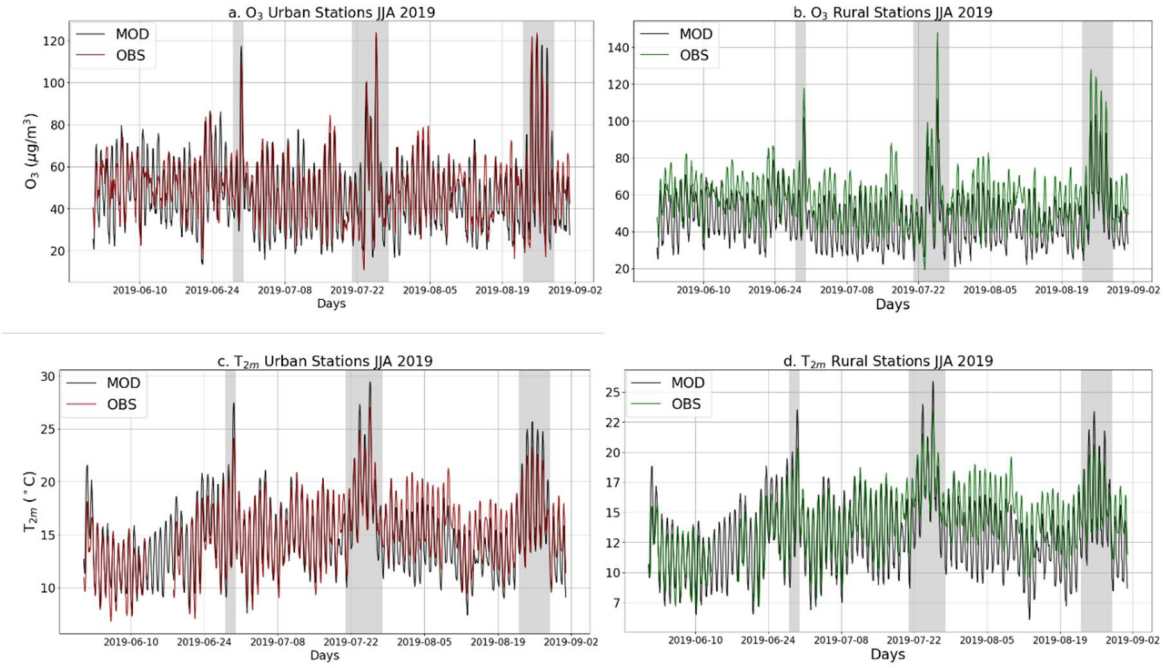

Figure S1. Hourly time series of observed and modelled (a, c) ozone (μg/m^3) and (c, d) surface temperature (°C) obtained by averaging across every urban background (left; in red) and rural background (right; green) AURN site. The time series covers the WRF-Chem simulation period (1st June to 31st August 2019). Model outputs (grey) shown for the BASE run and extracted at the same lat/lon location of the observations. Vertical grey areas highlight the HW periods.

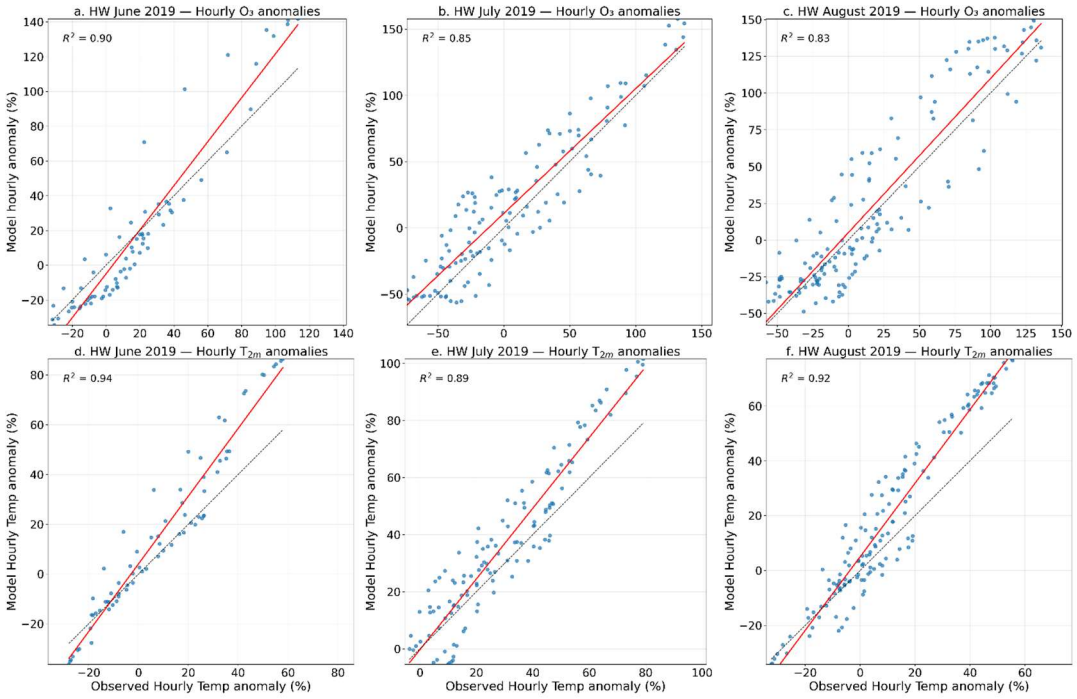

Figure S2. Scatter plot of observed versus modelled anomalies of (a-c) ozone (%), and (d-f) T_{2m} (%) for the HW periods of June, July and August 2019. Anomalies are calculated from hourly data as the difference between ozone or T_{2m} during HW periods relative to non-HW periods in each month. Linear regression lines and R^2 values are annotated. The dashed line is the 1:1 line.

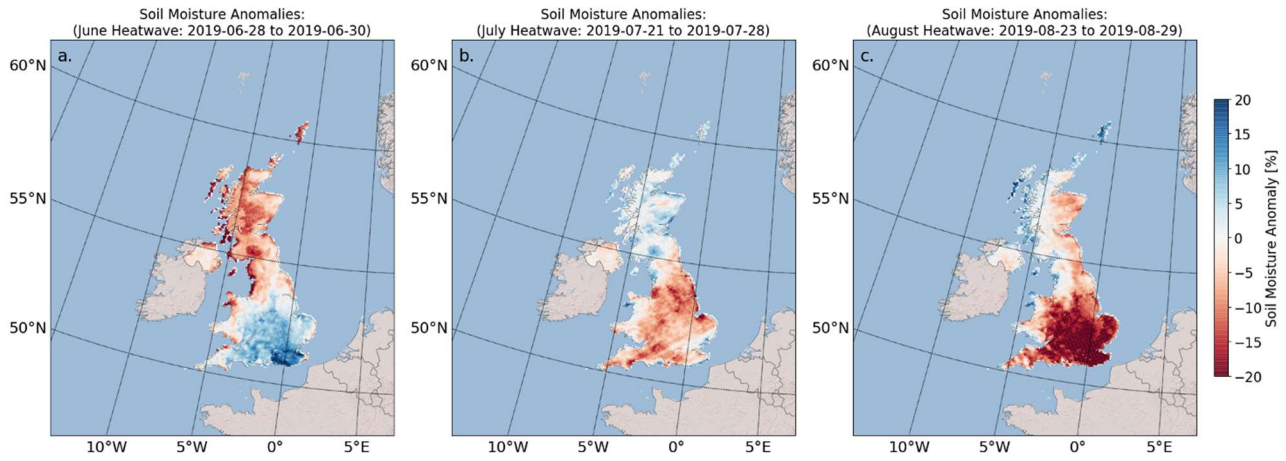

Figure S3. Soil moisture anomalies (%) from model outputs calculated between HW and non-HW periods for each month: (a) June, (b) July and (c) August 2019.

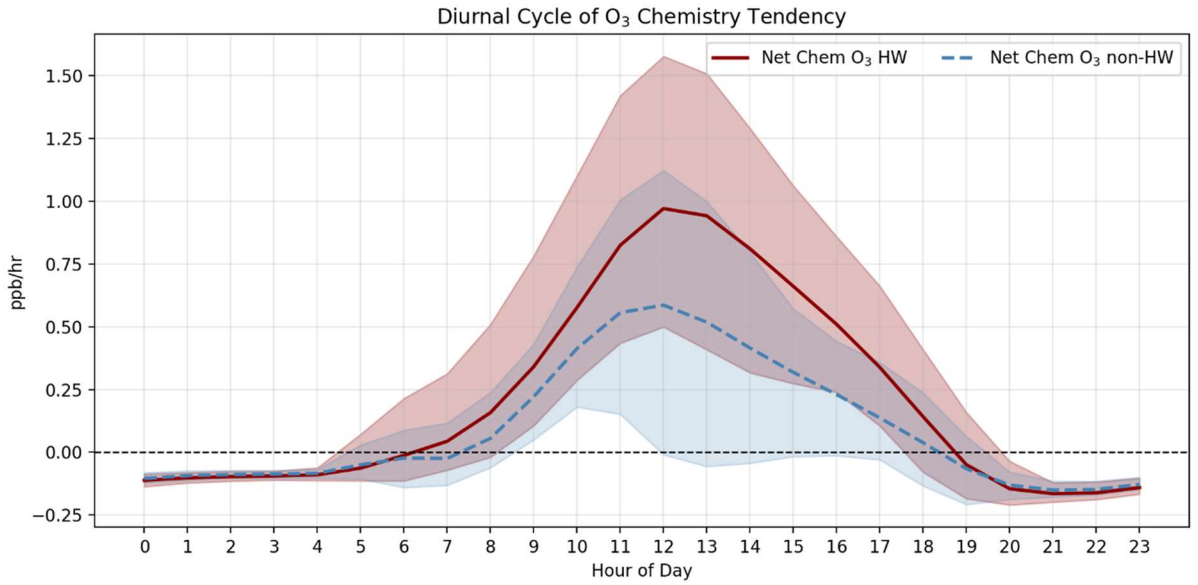

Figure S4. Modelled mean diurnal cycle of chemical net production (ppb/hr) during HW periods and non-HW periods of Summer 2019. The data are averaged across the entirety of the UK.

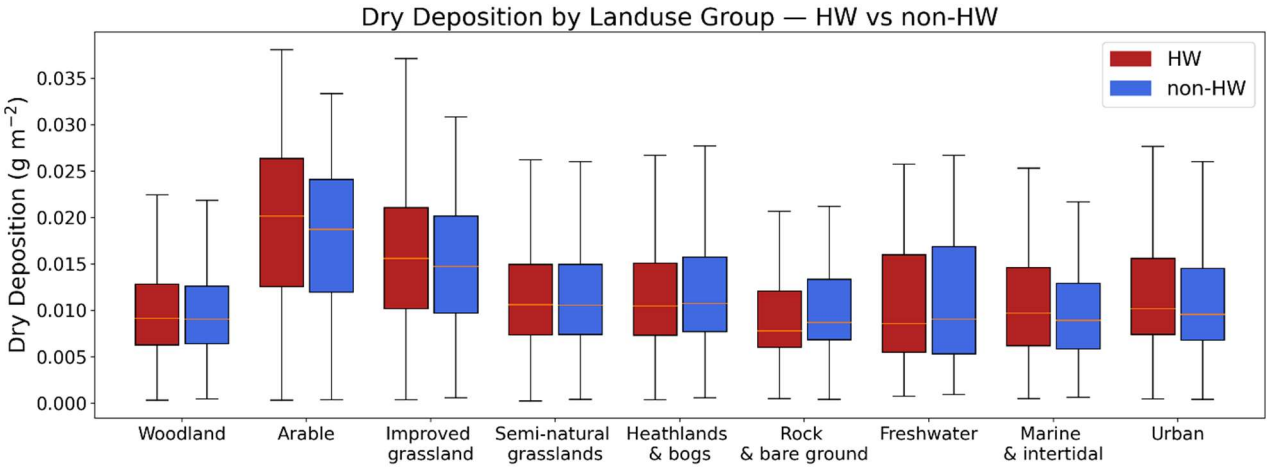

FigureS5: Dry deposition totals for the HW and non-HW periods calculated for the whole UK domain according to different grouped land-use categories.

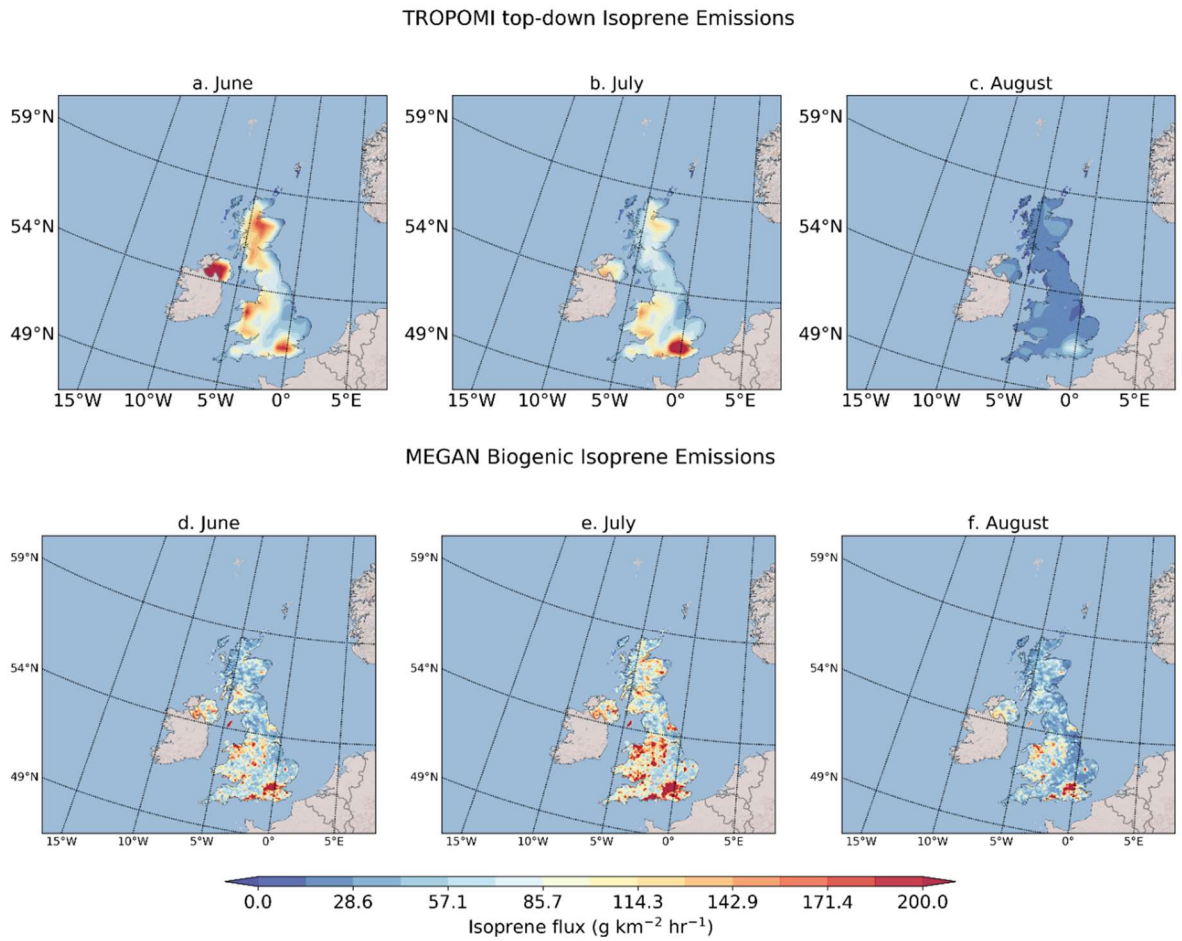

Figure S6: Estimates of biogenic isoprene emissions (g km^{-2} hr^{-1}) from (a-c) TROPOMI data with top-down approach [98] and MEGAN/WRF-chem (this study). The emissions are monthly means for Summer 2019.

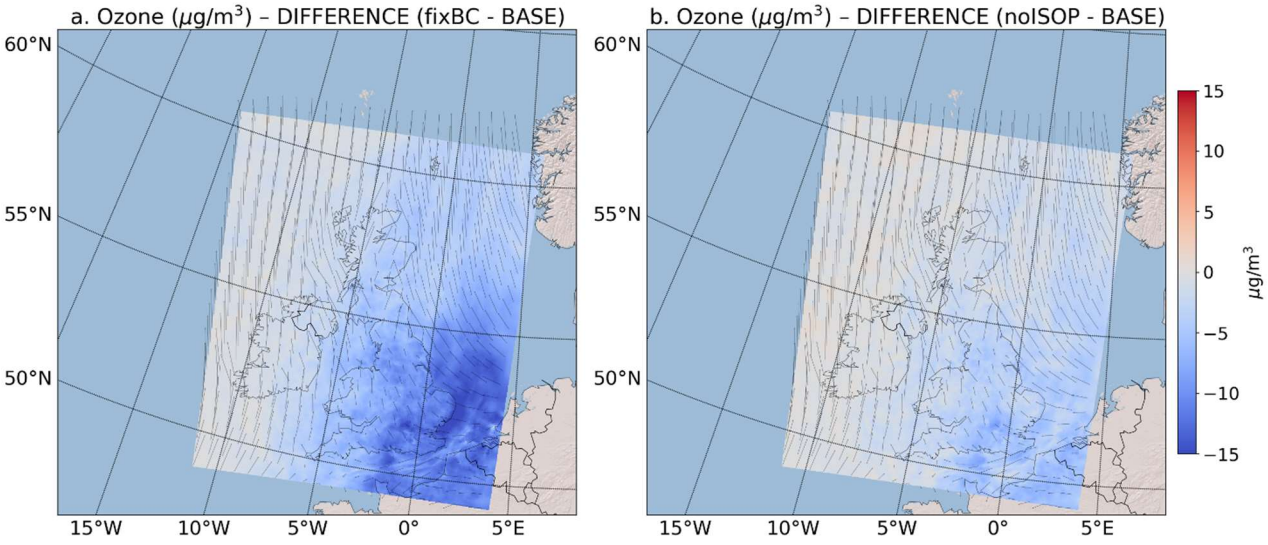

Figure S7. Difference in modelled MDA8 ozone (μg/m^3) between BASE run and runs (a) fixBC and (b) noISOP during all HW periods of June, July and August 2019.

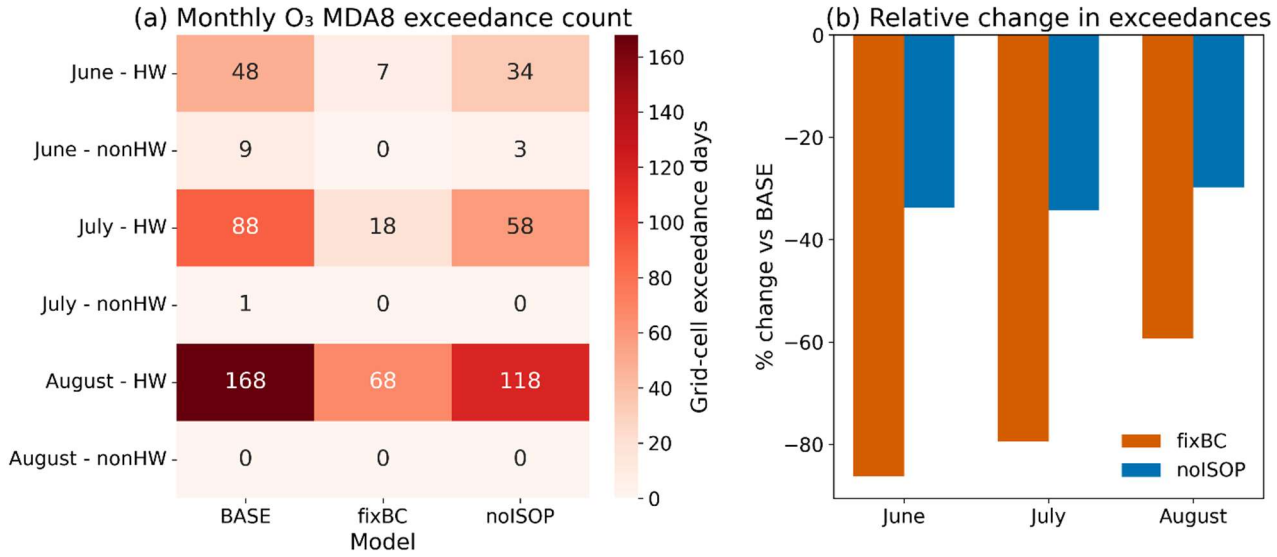

Figure S8. Combined assessment of O_3 MDA8 exceedances over June–August 2019. (a) Monthly exceedance count (MDA8 > 100 µg/m³) in grid-cell days, separated into HW (HW) and non-HW (non-HW) conditions for BASE, fixBC, and noISOP. (b) Percentage of UK grid cells exceeding the threshold and relative reductions under the two scenarios for each full monthly period.

Table S1: Heatwave periods during summer 2019 in the UK. Two criteria are used to assign these periods: (1) days when the mean Central England Temperature (CET) is in excess of 20°C; and (2) the Met Office criteria (MET) meaning that the maximum daily temperature exceeds a region-specific threshold for at least three consecutive days.

Period	Type	Max Temperature recorded (°C)
28th – 30th of June 2019	CET	34.0
21st – 28th of July 2019	MET	38.7
23rd – 29th of August 2019	MET	33.0

Table S2: Percentual change in emissions of biogenic isoprene and concentrations of ozone modelled by MEGANv2.0 and WRF-Chem. Totals calculated dividing the period of the heat waves by the normal period for each month and calculating the percentage of change of isoprene emissions and ozone concentrations between the two periods.

Emiss/Conc	Units	2019-06	2019-07	2019-08
Δ Isoprene Emissions	**(%)**	108.81	81.23	42.43
Δ Ozone Concentrations	**(%)**	13.10	28.0	36.81

References:

[1] MetOffice. *What is a heatwave?* 2023 [cited 2024 2024-12-12]; Available from: https://www.metoffice.gov.uk/weather/learn-about/weather/types-of-weather/temperature/heatwave.

[2] Arsad, F.S., et al., *The impact of heatwaves on mortality and morbidity and the associated vulnerability factors: a systematic review*. International Journal of Environmental Research and Public Health, 2022. **19**(23): p. 16356.

[3] Smale, D.A., et al., *Marine heatwaves threaten global biodiversity and the provision of ecosystem services*. Nature Climate Change, 2019. **9**(4): p. 306–312.

[4] Gao, M., et al., *Future intensification of co-occurrences of heat, PM2.5 and O3 extremes in China and India despite stringent air pollution controls*. Environmental Research Letters, 2025. **20**(1): p. 014044.

[5] Schnell, J.L. and M.J. Prather, *Co-occurrence of extremes in surface ozone, particulate matter, and temperature over eastern North America*. Proceedings of the National Academy of Sciences, 2017. **114**(11): p. 2854–2859.

[6] Perkins-Kirkpatrick, S. and S. Lewis, *Increasing trends in regional heatwaves*. Nature communications, 2020. **11**(1): p. 3357.

[7] IPCC, *Weather and Climate Extreme Events in a Changing Climate*, in *Climate Change 2021 – The Physical Science Basis: Working Group I Contribution to the Sixth Assessment Report of the Intergovernmental Panel on Climate Change*, C. Intergovernmental Panel on Climate, Editor. 2023, Cambridge University Press: Cambridge. p. 1513–1766.

[8] Doherty, R., et al., *Impacts of climate change on surface ozone and intercontinental ozone pollution: A multi-model study*. Journal of Geophysical Research: Atmospheres, 2013. **118**(9): p. 3744–3763.

[9] Wu, Y., et al., *Observation of heat wave effects on the urban air quality and PBL in New York City area*. Atmospheric Environment, 2019. **218**: p. 117024.

[10] Varotsos, K.V., C. Giannakopoulos, and M. Tombrou, *Ozone-temperature relationship during the 2003 and 2014 heatwaves in Europe*. Regional Environmental Change, 2019. **19**: p. 1653–1665.

[11] Li, M., et al., *Loss and recovery of vegetation productivity in response to extreme drought during 2022 across China*. Ecological Indicators, 2024. **166**: p. 112358.

[12] Soares, J., Plass, D., Kienzler, S., Gonzalez Ortiz, A., Gsella, A. and Horalek, J., *Assessing the environmental burden of disease related to air pollution in Europe in 2023. ETC HE Report 2025/8*, in *European Topic Centre on Human Health and the Environment*, A. European Environment, Editor. 2025.

[13] Bloomer, B.J., et al., *Observed relationships of ozone air pollution with temperature and emissions*. Geophysical Research Letters, 2009. **36**(9).

[14] Rasmussen, D., et al., *The ozone–climate penalty: past, present, and future*. Environmental science & technology, 2013. **47**(24): p. 14258–14266.

[15] Arneth, A., et al., *Clean the Air, Heat the Planet?* Science, 2009. **326**(5953): p. 672–673.

[16] Guion, A., et al., *Biogenic isoprene emissions, dry deposition velocity, and surface ozone concentration during summer droughts, heatwaves, and normal conditions in southwestern Europe*. Atmos. Chem. Phys., 2023. **23**(2): p. 1043–1071.

[17] Vieno, M., et al., *Modelling surface ozone during the 2003 heat-wave in the UK*. Atmospheric Chemistry and Physics, 2010. **10**(16): p. 7963–7978.

[18] Filleul, L., et al., *The relation between temperature, ozone, and mortality in nine French cities during the heat wave of 2003*. Environmental health perspectives, 2006. **114**(9): p. 1344–1347.

[19] Kahle, J.J., et al., *Interaction effects of temperature and ozone on lung function and markers of systemic inflammation, coagulation, and fibrinolysis: a crossover study of healthy young volunteers*. Environmental health perspectives, 2015. **123**(4): p. 310–316.
[20] Shi, W., et al., *Modification Effects of Temperature on the Ozone–Mortality Relationship: A Nationwide Multicounty Study in China*. Environmental Science & Technology, 2020. **54**(5): p. 2859–2868.
[21] Gouldsbrough, L., et al., *A machine learning approach to downscale EMEP4UK: analysis of UK ozone variability and trends*. EGUsphere, 2023. **2023**: p. 1–34.
[22] Finch, D.P. and P.I. Palmer, *Increasing ambient surface ozone levels over the UK accompanied by fewer extreme events*. Atmospheric Environment, 2020. **237**: p. 117627.
[23] AQEG. *Report: Ozone in the UK - Recent Trends and Future Projections*. 2021 [cited 2025 March]; Available from: https://uk-air.defra.gov.uk/library/reports.php?report_id=1064.
[24] Kalisa, E., et al., *Temperature and air pollution relationship during heatwaves in Birmingham, UK*. Sustainable Cities and Society, 2018. **43**: p. 111–120.
[25] Johnson, H., et al., *THE IMPACT OF THE 2003 HEAT WAVE ON MORTALITY AND HOSPITAL ADMISSIONS IN ENGLAND*. Epidemiology, 2004. **15**(4).
[26] Stedman, J.R., *The predicted number of air pollution related deaths in the UK during the August 2003 heatwave*. Atmospheric Environment, 2004. **38**(8): p. 1087–1090.
[27] Lee, J., et al., *Ozone photochemistry and elevated isoprene during the UK heatwave of august 2003*. Atmospheric Environment, 2006. **40**(39): p. 7598–7613.
[28] Francis, X.V., et al., *Mechanisms responsible for the build-up of ozone over South East England during the August 2003 heatwave*. Atmospheric Environment, 2011. **45**(38): p. 6880–6890.
[29] McCarthy, M., et al., *Drivers of the UK summer heatwave of 2018*. Weather (00431656), 2019. **74**(11).
[30] Pope, R.J., et al., *Investigation of the summer 2018 European ozone air pollution episodes using novel satellite data and modelling*. Atmos. Chem. Phys., 2023. **23**(20): p. 13235–13253.
[31] Otu-Larbi, F., et al., *Modelling the effect of the 2018 summer heatwave and drought on isoprene emissions in a UK woodland*. Glob Chang Biol, 2019.
[32] DEFRA, *Air Pollution in UK 2019*. 2020, Department for Environment Food & Rural Affairs
[33] MetOffice. *2019: a year in review*. 2020 [cited 2024 2024-12-12]; Available from: https://www.metoffice.gov.uk/about-us/news-and-media/media-centre/weather-and-climate-news/2019/weather-overview-2019.
[34] Grell, G.A., et al., *Fully coupled "online" chemistry within the WRF model*. Atmospheric Environment, 2005. **39**(37): p. 6957–6975.
[35] UKHSA. *Public health impacts of heat*. POST note 723 2024 [cited 2025 March]; Available from: https://post.parliament.uk/research-briefings/post-pn-0723/#:~:text=There%20is%20no%20universal%20definition,at%20least%2020%20%C2%B0C.
[36] MetOffice, *UK monthly climate summary June 2019*. 2019.
[37] PHE, *PHE heatwave mortality monitoring - Summer 2019*. 2019, Public Health of England.
[38] MetOffice, *2019 July Heatwave report*. 2019.
[39] MetOffice, *2019 August Heatwave report*. 2019.
[40] DEFRA. *Automatic Urban and Rural Network (AURN)*. 2019 [cited 2024 31/07/2024]; Available from: https://uk-air.defra.gov.uk/networks/network-info?view=aurn.

[41] MetOffice. *Met Office Integrated Data Archive System (MIDAS) Land and Marine Surface Stations Data (1853-current). NCAS British Atmospheric Data Centre*. 2012 May 2024]; Available from: http://catalogue.ceda.ac.uk/uuid/220a65615218d5c9cc9e4785a3234bd0.

[42] Hembeck, L., et al., *Investigation of the Community Multiscale air quality (CMAQ) model representation of the Climate Penalty Factor (CPF)*. Atmospheric Environment, 2022. **283**.

[43] Fast, J.D., et al., *Evolution of ozone, particulates, and aerosol direct radiative forcing in the vicinity of Houston using a fully coupled meteorology-chemistry-aerosol model*. Journal of Geophysical Research: Atmospheres, 2006. **111**(D21).

[44] Gupta, P., et al., *WRF-Chem modeling study of heat wave driven ozone over southeast region, India*. Environmental Pollution, 2024. **340**: p. 122744.

[45] Yim, S.H., J.C. Fung, and A.K. Lau, *Use of high-resolution MM5/CALMET/CALPUFF system: SO2 apportionment to air quality in Hong Kong*. Atmospheric Environment, 2010. **44**(38): p. 4850–4858.

[46] Crippa, P., et al., *The impact of resolution on meteorological, chemical and aerosol properties in regional simulations with WRF-Chem*. Atmospheric Chemistry and Physics, 2017. **17**(2): p. 1511–1528.

[47] Stockwell, W.R., et al., *The second generation regional acid deposition model chemical mechanism for regional air quality modeling*. Journal of Geophysical Research: Atmospheres, 1990. **95**(D10): p. 16343–16367.

[48] Tuccella, P., et al., *Modeling of gas and aerosol with WRF/Chem over Europe: Evaluation and sensitivity study*. Journal of Geophysical Research: Atmospheres, 2012. **117**(D3).

[49] Mar, K.A., et al., *Ozone air quality simulations with WRF-Chem (v3.5.1) over Europe: model evaluation and chemical mechanism comparison*. Geoscientific Model Development, 2016. **9**(10): p. 3699–3728.

[50] Balzarini, A., et al., *WRF-Chem model sensitivity to chemical mechanisms choice in reconstructing aerosol optical properties*. Atmospheric Environment, 2015. **115**: p. 604–619.

[51] Rogers, E., et al., *Changes to the NCEP Meso Eta Analysis and Forecast System: Increase in resolution, new cloud microphysics, modified precipitation assimilation, modified 3DVAR analysis*. NWS Technical Procedures Bulletin, 2001. **488**: p. 15.

[52] Tewari, M., F. Chen, W. Wang, J. Dudhia, M. A. LeMone, K. Mitchell, M. Ek, G. Gayno, J. Wegiel, and R. H. Cuenca,, *Implementation and verification of the unified NOAH land surface model in the WRF model. InProceedings of the 20th Conference on Weather Analysis and Forecasting*, in *16th Conference on Numerical Weather Prediction*. 2004: Seattle. p. 11–15.

[53] Grell, G.A. and D. Dévényi, *A generalized approach to parameterizing convection combining ensemble and data assimilation techniques*. Geophysical Research Letters, 2002. **29**(14): p. 38–1–38–4.

[54] Janić, Z.I., *Nonsingular implementation of the Mellor-Yamada level 2.5 scheme in the NCEP Meso model*. 2001.

[55] Janjić, Z.I., *The step-mountain eta coordinate model: Further developments of the convection, viscous sublayer, and turbulence closure schemes*. Monthly weather review, 1994. **122**(5): p. 927–945.

[56] Mesinger, F., *Forecasting upper tropospheric turbulence within the framework of the Mellor-Yamada 2.5 closure*. Res. Activ. Atmos. Oceanic Mod., 1993.

[57] Chou, M.-D. and M.J. Suarez, *An efficient thermal infrared radiation parameterization for use in general circulation models*. 1994.

[58] Iacono, M.J., et al., *Radiative forcing by long-lived greenhouse gases: Calculations with the AER radiative transfer models*. Journal of Geophysical Research: Atmospheres, 2008. **113**(D13).
[59] Salamanca, F. and A. Martilli, *A new building energy model coupled with an urban canopy parameterization for urban climate simulations—Part II. Validation with one dimension off-line simulations*. Theoretical and Applied Climatology, 2010. **99**: p. 345–356.
[60] NCAR, *ERA5 Reanalysis (0.25 Degree Latitude-Longitude Grid)*. 2019, Research Data Archive at the National Center for Atmospheric Research, Computational and Information Systems Laboratory: Boulder, CO.
[61] Buchholz, R.R., Emmons, L. K., Tilmes, S., & The CESM2 Development Team. *CESM2.1/CAM-chem Instantaneous Output for Boundary Conditions*. *UCAR/NCAR* 2019 October 2023]; subset used for year 2019, Lat: 30 to 65, Lon: 160 to 210].
[62] Liu, Y., et al., *The operational mesogamma-scale analysis and forecast system of the US Army Test and Evaluation Command. Part I: Overview of the modeling system, the forecast products, and how the products are used*. Journal of Applied Meteorology and Climatology, 2008. **47**(4): p. 1077–1092.
[63] NAEI, N.A.E.I. *National Atmospheric Emission Inventory for UK*. 2021 [cited 2021 May 2021]; Available from: https://naei.beis.gov.uk/.
[64] Guenther, A., et al., *The Model of Emissions of Gases and Aerosols from Nature version 2.1 (MEGAN2. 1): an extended and updated framework for modeling biogenic emissions*. Geoscientific Model Development, 2012. **5**(6): p. 1471–1492.
[65] Wiedinmyer, C. and L. Emmons, *Fire Inventory from NCAR version 2 Fire Emission*. 2022, Research Data Archive at the National Center for Atmospheric Research, Computational and Information Systems Laboratory: Boulder, CO.
[66] Francis, X.S., R., *CMAQ Development for UK National Modelling: Technical Report on the Influence of Boundary Conditions on Regional Air. 2013*. 2013.
[67] Emmons, L.K., et al., *The Chemistry Mechanism in the Community Earth System Model Version 2 (CESM2)*. Journal of Advances in Modeling Earth Systems, 2020. **12**(4): p. e2019MS001882.
[68] Jeffries, H.E. and S. Tonnesen, *A comparison of two photochemical reaction mechanisms using mass balance and process analysis*. Atmospheric Environment, 1994. **28**(18): p. 2991–3003.
[69] Xiang, Y., et al., *Elucidating the ozone formation and transport mechanism in the Pearl River Delta against the backdrop of heatwave*. Environmental Research Letters, 2025. **20**(7): p. 074040.
[70] Granier, C., et al., *The Copernicus atmosphere monitoring service global and regional emissions (April 2019 version)*. 2019, Copernicus Atmosphere Monitoring Service.
[71] SNAP. *UN/ECE Classification of Emission Sources* 1994; Available from: https://uk-air.defra.gov.uk/assets/documents/reports/empire/naei/annreport/annrep98/naeiapp4.html.
[72] Guevara, M., et al., *HERMESv3, a stand-alone multi-scale atmospheric emission modelling framework – Part 1: global and regional module*. Geoscientific Model Development, 2019. **12**(5): p. 1885–1907.
[73] Guevara, M., et al., *HERMESv3, a stand-alone multi-scale atmospheric emission modelling framework – Part 2: The bottom–up module*. Geoscientific Model Development, 2020. **13**(3): p. 873–903.
[74] Achebak, H., et al., *Geographic sources of ozone air pollution and mortality burden in Europe*. Nature Medicine, 2024. **30**(6): p. 1732–1738.

[75] Ferreira, J., et al., *A comparative analysis of two highly spatially resolved European atmospheric emission inventories*. Atmospheric Environment, 2013. **75**: p. 43–57.
[76] Guevara, M., et al., *An improved system for modelling Spanish emissions: HERMESv2. 0*. Atmospheric environment, 2013. **81**: p. 209–221.
[77] Seemann, S.-L., et al., *Combining the Emission Preprocessor HERMES with the Chemical Transport Model TM5-MP*. Atmosphere, 2024. **15**(4): p. 469.
[78] Guevara, M., et al., *An emission processing system for air quality modelling in the Mexico City metropolitan area: Evaluation and comparison of the MOBILE6.2-Mexico and MOVES-Mexico traffic emissions*. Science of The Total Environment, 2017. **584-585**: p. 882–900.
[79] Rodriguez-Rey, D., et al., *A coupled macroscopic traffic and pollutant emission modelling system for Barcelona*. Transportation Research Part D: Transport and Environment, 2021. **92**: p. 102725.
[80] Soret, A., et al. *Status and Future Vision of the CALIOPE Air Quality Forecasting System: Support for Air Quality Policies*. in *International Technical Meeting on Air Pollution Modelling and its Application*. 2021. Springer.
[81] Guenther, A., et al., *Estimates of global terrestrial isoprene emissions using MEGAN (Model of Emissions of Gases and Aerosols from Nature)*. Atmos. Chem. Phys., 2006. **6**(11): p. 3181–3210.
[82] Huang, L., et al., *Recommendations on benchmarks for numerical air quality model applications in China–Part 2: Ozone and uncertainty analysis*. Atmospheric Chemistry and Physics, 2025. **25**(7): p. 4233–4249.
[83] Boylan, J.W. and A.G. Russell, *PM and light extinction model performance metrics, goals, and criteria for three-dimensional air quality models*. Atmospheric Environment, 2006. **40**(26): p. 4946–4959.
[84] Kelly, J.M., et al., *The impact of biogenic, anthropogenic, and biomass burning volatile organic compound emissions on regional and seasonal variations in secondary organic aerosol*. Atmospheric Chemistry and Physics, 2018. **18**(10): p. 7393–7422.
[85] Lefohn, A.S., et al., *Tropospheric ozone assessment report: Global ozone metrics for climate change, human health, and crop/ecosystem research*. Elem Sci Anth, 2018. **6**: p. 27.
[86] DEFRA, *Update on Implementation of the Daily Air Quality Index*. 2013.
[87] WHO, *Air quality guidelines: global update 2005: particulate matter, ozone, nitrogen dioxide and sulfur dioxide*. , W.H.O.R.O.f. Europe, Editor. 2006.
[88] Archer-Nicholls, S., et al., *Gaseous chemistry and aerosol mechanism developments for version 3.5.1 of the online regional model, WRF-Chem*. Geoscientific Model Development, 2014. **7**(6): p. 2557–2579.
[89] Lupaşcu, A., et al., *Attribution of surface ozone to NOx and volatile organic compound sources during two different high ozone events*. Atmos. Chem. Phys., 2022. **22**(17): p. 11675–11699.
[90] Beobide-Arsuaga, G., et al., *Spring Regional Sea Surface Temperatures as a Precursor of European Summer Heatwaves*. Geophysical Research Letters, 2023. **50**(2): p. e2022GL100727.
[91] Otero, N., et al., *The impact of atmospheric blocking on the compounding effect of ozone pollution and temperature: a copula-based approach*. Atmospheric Chemistry and Physics, 2022. **22**(3): p. 1905–1919.
[92] Coyle, M., R. Smith, and D. Fowler, *An ozone budget for the UK: using measurements from the national ozone monitoring network; measured and modelled meteorological*

data, and a 'big-leaf'resistance analogy model of dry deposition. Environmental Pollution, 2003. **123**(1): p. 115–123.
[93] UKCEH, *Land Cover Map 2019*, N.E.R.C.A. NE/R016429/1, Editor. 2019.
[94] Seco, R., et al., *Volatile organic compound fluxes in a subarctic peatland and lake*. Atmos. Chem. Phys., 2020. **20**(21): p. 13399–13416.
[95] Guenther, A., et al., *Estimates of global terrestrial isoprene emissions using MEGAN (Model of Emissions of Gases and Aerosols from Nature)*. Atmos. Chem. Phys, 2006. **6**: p. 3181–3210.
[96] Ferracci, V., et al., *Continuous Isoprene Measurements in a UK Temperate Forest for a Whole Growing Season: Effects of Drought Stress During the 2018 Heatwave*. Geophysical Research Letters, 2020. **47**(15).
[97] Wang, H., et al., *Modeling Isoprene Emission Response to Drought and Heatwaves Within MEGAN Using Evapotranspiration Data and by Coupling With the Community Land Model*. J Adv Model Earth Syst, 2022. **14**(12): p. e2022MS003174.
[98] Oomen, G.M., et al., *Weekly derived top-down volatile-organic-compound fluxes over Europe from TROPOMI HCHO data from 2018 to 2021*. Atmos. Chem. Phys., 2024. **24**(1): p. 449–474.
[99] Hong, Q., et al., *Evaluating the feasibility of formaldehyde derived from hyperspectral remote sensing as a proxy for volatile organic compounds*. Atmospheric Research, 2021. **264**: p. 105777.
[100] Trimmel, H., et al., *The influence of vegetation drought stress on formaldehyde and ozone distributions over a central European city*. Atmospheric Environment, 2023. **304**: p. 119768.
[101] Sun, L., et al., *Impacts of meteorology and emissions on summertime surface ozone increases over central eastern China between 2003 and 2015*. Atmos. Chem. Phys., 2019. **19**(3): p. 1455–1469.
[102] Kiefer, M.T., et al., *Evaluation of the ventilation index in complex terrain: A dispersion modeling study*. Journal of Applied Meteorology and Climatology, 2019. **58**(3): p. 551–568.
[103] Jeong, S., et al., *Role of air stagnation in determining daily average PM2.5 concentrations in areas with significant impact of long-range transport*. Atmospheric Pollution Research, 2024. **15**(7): p. 102147.
[104] Mukhopadhyay, K., et al., *Use of ventilation-index in the development of exposure model for indoor air pollution—A review*. Open Journal of Air Pollution, 2014. **3**(3): p. 33–41.
[105] Vannucci, P.F. and R.C. Cohen, *Temperature-Dependent Nighttime Stagnation Episodes Driving Decadal Air Pollutant Exceedances in Los Angeles*. ACS ES&T Air, 2024. **1**(6): p. 474–480.
[106] Menut, L., et al., *Sensitivity of photochemical pollution using the adjoint of a simplified chemistry-transport model*. Journal of Geophysical Research: Atmospheres, 2000. **105**(D12): p. 15379–15402.
[107] Romero-Alvarez, J., et al., *Sources of surface O3 in the UK: tagging O3 within WRF-Chem*. Atmospheric Chemistry and Physics, 2022. **22**(20): p. 13797–13815.
[108] Xu, P., et al., *The record-breaking heat wave of June 2019 in Central Europe*. Atmospheric Science Letters, 2020. **21**(4): p. e964.
[109] Vautard, R., et al., *Human contribution to the record-breaking June and July 2019 heatwaves in Western Europe*. Environmental Research Letters, 2020. **15**(9): p. 094077.

[110] Sousa, P.M., et al., *Distinct influences of large-scale circulation and regional feedbacks in two exceptional 2019 European heatwaves*. Communications Earth & Environment, 2020. **1**(1): p. 48.